Modern Physics Letters B
Vol. 39, No. 21 (2025) 2550060 (27 pages)

DOI: 10.1142/S0217984925500605

Integrability and multiple-rogue and multi-soliton wave solutions of the $(3+1)$-dimensional Hirota–Satsuma–Ito equation

Jingyi Chu and Yaqing Liu*
School of Applied Science,
Beijing Information Science and Technology University,
Beijing 100192, China
**liuyaqing1981@163.com*

Wen-Xiu Ma†
Department of Mathematics, Zhejiang Normal University,
Jinhua 321004, China
Department of Mathematics, King Abdulaziz University,
Jeddah 21589, Saudi Arabia
Department of Mathematics and Statistics,
University of South Florida, Tampa, FL 33620-5700, USA
Material Science Innovation and Modelling,
Department of Mathematical Science, North-West University,
Mafikeng Campus, Mmabatho 2735, South Africa
mawx@cas.usf.edu

Received 4 July 2024
Revised 13 August 2024
Accepted 11 September 2024
Published 30 November 2024

This paper constructs a new $(3+1)$-dimensional Hirota–Satsuma–Ito equation and employs the Hirota N-soliton condition to determine the conditions for the existence of N-soliton solutions. Under these conditions, the Hirota bilinear method is utilized to derive N-soliton solutions of the equation. Additionally, breather solutions of the equation are obtained through constraints on complex conjugate parameters, while lump solutions are derived using the long-wave limit method. Building upon these results, interaction solutions are also explored. Furthermore, through the multiple-rogue wave method, multi-rogue wave solutions of the $(3+1)$-dimensional Hirota–Satsuma–Ito equation are investigated. A comparison between lump solutions obtained via the Hirota bilinear method and the multi-rogue wave solutions from multiple-rogue wave method reveals significant discrepancies.

Keywords: $(3+1)$-dimensional Hirota–Satsuma–Ito equation; Hirota N-soliton condition; Hirota bilinear method; multi-rogue wave solutions.

PACS Nos.: 02.30.Ik, 47.35.Fg

†Corresponding author.

1. Introduction

The soliton theory emerged in the 1960s while exploring solutions to nonlinear partial differential equations (NPDEs), notably originating from the study of the Korteweg–de Vries (KdV) equation. Initially applied to water wave theory, the KdV equation aimed to model one-dimensional water wave evolution. Within it, researchers discovered a remarkable phenomenon: a unique class of solutions termed "solitary waves" or "solitons", resembling single wave packets. This discovery sparked widespread interest among mathematicians and physicists. Solitons revolutionized the approach to solving NPDEs and profoundly impacted various mathematical and physical disciplines. In mathematics, they led to investigations into completely integrable systems, offering analytical solutions to previously intractable problems. In physics, solitons provided solutions to formerly unsolvable NPDEs, thus addressing practical challenges. Over time, soliton theory diversified, giving rise to various solution methodologies, including the inverse scattering method,[1–4] the Riemann–Hilbert method,[5–7] the Darboux transformation method,[8,9] the Hirota bilinear method,[10–13] Bäcklund transformation,[14–17] and others. These methods played crucial roles in constructing exact solutions and studying integrable systems.

Among these methods, the Hirota bilinear method is renowned for its widespread application due to its simplicity and effectiveness. This mathematical technique is specifically designed for tackling NPDEs. It operates by utilizing a bilinear operator to convert the given NPDE into a bilinear form. Subsequently, a series of recursion relations are applied to derive functional representations of solitons. The essence of the Hirota bilinear method lies in the introduction and utilization of the Hirota bilinear operator, elucidated in detail in Ref. 10. The operator is defined as follows:

$$\begin{aligned} D_x^m D_y^n D_z^r D_t^p (f\cdot g) = {} & (\partial_x - \partial_{x'})^m (\partial_y - \partial_{y'})^n (\partial_z - \partial_{z'})^r (\partial_t - \partial_{t'})^p \\ & \cdot f(x,y,z,t) g(x',y',z',t')|_{x=x',y=y',z=z',t=t'}. \end{aligned} \tag{1}$$

In particular, we have

$$D_x f\cdot g = f_x g - f g_x, \quad D_x^2 f\cdot g = f_{xx} g - 2 f_x g_x + f g_{xx}. \tag{2}$$

When $f = g$, the Hirota bilinear expression is

$$\begin{aligned} D_x^m D_y^n D_z^r D_t^p (f\cdot f) = {} & (\partial_x - \partial_{x'})^m (\partial_y - \partial_{y'})^n (\partial_z - \partial_{z'})^r (\partial_t - \partial_{t'})^p \\ & \cdot f(x,y,z,t) f(x',y',z',t')|_{x=x',y=y',z=z',t=t'}, \end{aligned} \tag{3}$$

and

$$D_x f\cdot f = 0, \quad D_x^2 f\cdot f = 2(f_{xx} f - f_x^2). \tag{4}$$

Therefore, it can be observed that odd-order Hirota bilinear expressions are all equal to 0. Let $\mathcal{P}(x,y,z,t)$ be an even-degree polynomial, with $\mathcal{P}(\mathbf{0}) = \mathcal{P}(0,0,0,0) = 0$, which means it does not contain constant terms. The related Hirota bilinear equations are defined as follows:

$$\mathcal{P}(D_{x_1}, D_{x_2}, \ldots, D_{x_M}) f\cdot f = 0, \tag{5}$$

where each term is a Hirota bilinear expression. If an NPDE can be converted into a Hirota bilinear equation through a transformation of its dependent variables, it is classified as possessing a Hirota bilinear representation.

The Hirota–Satsuma (HS) equation, introduced by Hirota and Satsuma,[18] models the propagation of unidirectional shallow water waves. It consists of the following system:

$$\begin{cases} u_t = u_{xxt} - 3u_x v_t + 3uu_t - u_x, \\ v_x = -u, \end{cases} \tag{6}$$

where $u = u(x,t)$ and $v = v(x,t)$ represent the wave amplitudes as functions of the scaled spatial variable x and temporal variable t. In Ref. 19, Ito provided the bilinear from the HS equation (6) as an illustration of the modified KdV (mKdV)-type equation.

To extend the $(1+1)$-dimensional HS equation (6) to integrable $(2+1)$-dimension, the Hirota–Satsuma–Ito (HSI) equation[20] is introduced as follows:

$$\begin{cases} w_t = u_{xxt} - 3u_x v_t + 3uu_t + \alpha u_x, \\ w_x = -u_y, \\ v_x = -u, \end{cases} \tag{7}$$

where u represents the field function, while v and w are potentials of field function derivatives, with $\alpha = \pm 1$. In recent years, numerous scholars have explored various exact solutions for the HSI equation (7). For example, Zhou *et al.*[21] employed symbolic computation to obtain lump and lump-soliton solutions. An and Guo[22] utilized the Hirota bilinear method to study N-soliton solutions, breather solutions, lump solutions, and nonlinear transformation waves for the HSI equation (7). Building upon the N-soliton solutions, Shen *et al.*[23] constructed X-type solitons and resonant Y-type solitons. Liu *et al.*[24] analyzed the asymptotic behaviors of two-soliton solutions and two types of semi-rational solutions. Additionally, some researchers have extended the HSI equation (7). For instance, Liu *et al.*[25] modified the HSI equation (7) to derive the $(2+1)$-dimensional generalized HSI equation. Wu and Tian[26] further studied the structural solutions of this new equation and discussed the dynamical characteristics of nonlinear waves under transformations. Chen *et al.*[27] formulated a variable-coefficient HSI equation and investigated its N-soliton solutions.

Expanding our investigation to the $(3+1)$-dimensional realm, we present the extended form of the HSI equation as follows:

$$\begin{cases} \alpha p_t + u_{xxt} + 3(uw)_x + \beta q_z = 0, \\ u_t = w_x, \\ u_y = p_x, \\ u_z = q_x. \end{cases} \tag{8}$$

Here, α and β are constants, while $u = u(x,y,z,t)$, $p = p(x,y,z,t)$, $w = w(x,y,z,t)$, and $q = q(x,y,z,t)$ represent the wave amplitudes, varying with scaled spatial variables x, y, z and the temporal variable t. Introducing a logarithmic transformation to the $(3+1)$-dimensional HSI equation (8), defined as follows:

$$u = 2(\ln f)_{xx}, \quad p = 2(\ln f)_{xy}, \quad w = 2(\ln f)_{xt}, \quad q = 2(\ln f)_{xz}, \tag{9}$$

it has a Hirota bilinear form as

$$\mathcal{P}(D_x, D_y, D_z, D_t) f \cdot f = (\alpha D_y D_t + D_x^3 D_t + \beta D_z^2) f \cdot f = 0, \tag{10}$$

resulting in the Hirota bilinear equation

$$\mathcal{P}(x, y, z, t) = x^3 t + \alpha y t + \beta z^2 = 0. \tag{11}$$

Despite the non-integrability of the $(3+1)$-dimensional general HSI equation, as outlined in Ref. 28, two integrable conditions have been identified through Painlevé integrability analysis. Similarly, our newly constructed $(3+1)$-dimensional HSI equation (8) follows suit. We will employ the Hirota N-soliton condition to discern the existence criteria for three-soliton solutions, as the presence of three solitons typically signifies integrability of the equation. The Hirota N-soliton condition was first introduced by Hirota.[10] In 1986, Newell and Yunbo[29] provided a comprehensive discussion on this topic. Subsequently, Hietarinta[30–33] elaborated on the condition using the language of algebraic geometry. In 2011, Ma[34] investigated the three-soliton condition for the $(3+1)$-dimensional Kadomtsev–Petviashvili (KP) equation and conducted further research in this domain.[35–40] This paper aims to derive the N-soliton solutions, breather solutions, lump solutions, and interaction solutions of the $(3+1)$-dimensional HSI equation (8) through the Hirota bilinear method, along with multi-rogue solutions via multiple-rogue wave method.

The structure of this paper is delineated as follows. In Sec. 2, the presentation of the N-soliton solutions for the $(3+1)$-dimensional HSI equation (8) is explored using the Hirota bilinear method, alongside the establishment of conditions for the existence of these solitons based on the Hirota N-soliton conditions. In Sec. 3, further development of the N-soliton expressions introduced in Sec. 2 is conducted, with solutions derived for soliton solutions, breather solutions, lump solutions, and their interaction solutions. In Sec. 4, multiple-rogue wave method is applied to obtain multi-rogue wave solutions of the $(3+1)$-dimensional HSI equation (8) controlled by wave centers (θ, δ). Finally, a summary of the findings is presented.

2. Integrability Condition and Multi-Soliton Solutions

The N-soliton solutions for the $(3+1)$-dimensional HSI equation (8) are analyzed, and the corresponding N-soliton condition is derived. The existence of N-soliton solutions indicates the integrability of the equation. The Hirota N-soliton condition[34–38] is pivotal in ascertaining the existence of such solutions.

2.1. *N-soliton condition*

To investigate the existence of N-soliton solutions for Eq. (8), it is necessary to identify N-wave vectors, denoted as

$$\mathbf{v}_i = (a_i, b_i, c_i, d_i), \quad 1 \le i \le N, \tag{12}$$

where a_i, b_i, c_i, d_i are constants. Next, we introduce the following definition:

$$\mathcal{H}(\mathbf{v}_1, \ldots, \mathbf{v}_n) = \sum_{\sigma=\pm 1} \mathcal{P}\left(\sum_{r=1}^{n} \sigma_r \mathbf{v}_r\right) \prod_{1\le r<s\le n} \mathcal{P}(\sigma_r \mathbf{v}_r - \sigma_s \mathbf{v}_s)\sigma_r \sigma_s, \tag{13}$$

where $\sigma = (\sigma_1, \sigma_2, \ldots, \sigma_n)$, and $\sigma = \pm 1$ indicates that each σ_i takes the values of 1 or -1, $1 \le n \le N$. If $\mathcal{H}(\mathbf{v}_1, \ldots, \mathbf{v}_n) = 0$, it signifies that the $(3+1)$-dimensional HSI equation (8) accommodates N-soliton solutions. Conversely, if $\mathcal{H}(\mathbf{v}_1, \ldots, \mathbf{v}_n) \ne 0$, the equation does not admit N-soliton solutions. This criterion acts as a pivotal determinant for the existence of N-soliton solutions, thereby underscoring the integrability of the equation.

For $N = 1$, the emergence of a one-soliton solution is contingent upon $\mathcal{H}(\mathbf{v}_1) = \mathcal{P}(\mathbf{v}_1) + \mathcal{P}(-\mathbf{v}_1) = 2\mathcal{P}(\mathbf{v}_1)$, which results in the dispersion relation $\mathcal{P}(\mathbf{v}_1) = 0$, or equivalently, $d_i = -\frac{\beta c_i^2}{a_i^3 + \alpha b_i}$ for $1 \le i \le N$. The assumption that the dispersion relation holds is rooted in $\mathcal{P}$ being an even polynomial, as discussed in (4).

For $N = 2$, the existence of a two-soliton solution is governed by the condition given in (13)

$$\mathcal{H}(\mathbf{v}_1, \mathbf{v}_2) = 2\mathcal{P}(\mathbf{v}_1 - \mathbf{v}_2)(\mathcal{P}(\mathbf{v}_1 + \mathbf{v}_2) - \mathcal{P}(\mathbf{v}_1 + \mathbf{v}_2))\mathcal{P}(\mathbf{v}_1 - \mathbf{v}_2) = 0, \tag{14}$$

which holds as an identity. This condition unequivocally indicates the perpetual existence of two-soliton solutions.

For $N = 3$, the requisite condition for a three-soliton solution is

$$\begin{aligned}\sum_{\sigma_1,\sigma_2,\sigma_3=\pm 1} &\mathcal{P}(\sigma_1 \mathbf{v}_1 + \sigma_2 \mathbf{v}_2 + \sigma_3 \mathbf{v}_3)\mathcal{P}(\sigma_1 \mathbf{v}_1 - \sigma_2 \mathbf{v}_2) \\ &\cdot \mathcal{P}(\sigma_2 \mathbf{v}_2 - \sigma_3 \mathbf{v}_3)\mathcal{P}(\sigma_1 \mathbf{v}_1 - \sigma_3 \mathbf{v}_3) = 0.\end{aligned} \tag{15}$$

It is widely acknowledged that the existence of three-soliton solutions often implies the existence of N-soliton solutions. The presence of three-soliton solutions is frequently indicative of the equation's integrability. Therefore, the three-soliton condition (15) for Eq. (10) can be rewritten as

$$\begin{aligned}&\sum_{\sigma_1,\sigma_2,\sigma_3=\pm 1} \mathcal{P}(\sigma_1 \mathbf{v}_1 + \sigma_2 \mathbf{v}_2 + \sigma_3 \mathbf{v}_3)\mathcal{P}(\sigma_1 \mathbf{v}_1 - \sigma_2 \mathbf{v}_2)\mathcal{P}(\sigma_2 \mathbf{v}_2 - \sigma_3 \mathbf{v}_3)\mathcal{P}(\sigma_1 \mathbf{v}_1 - \sigma_3 \mathbf{v}_3) \\ &\quad = 2 \sum_{(\sigma_1,\sigma_2,\sigma_3)\in S} \mathcal{P}(\sigma_1 \mathbf{v}_1 + \sigma_2 \mathbf{v}_2 + \sigma_3 \mathbf{v}_3)\mathcal{P}(\sigma_1 \mathbf{v}_1 - \sigma_2 \mathbf{v}_2)\mathcal{P}(\sigma_2 \mathbf{v}_2 - \sigma_3 \mathbf{v}_3)\mathcal{P}(\sigma_1 \mathbf{v}_1 - \sigma_3 \mathbf{v}_3)\end{aligned}$$

$$
\begin{aligned}
&= \frac{144\beta^4 a_1a_2a_3}{(a_1^3+\alpha b_1)^3(a_2^3+\alpha b_2)^3(a_3^3+\alpha b_3)^3}\left\{\alpha^2\begin{vmatrix} a_1b_1 & b_1c_1 & c_1^2 \\ a_2b_2 & b_2c_2 & c_2^2 \\ a_2b_3 & b_3c_3 & c_3^2\end{vmatrix} + \alpha\begin{vmatrix} a_1^4 & b_1c_1 & c_1^2 \\ a_2^4 & b_2c_2 & c_2^2 \\ a_3^4 & b_2c_3 & c_3^2\end{vmatrix}\right.\\
&\quad\left. -\alpha\begin{vmatrix} a_1^3c_1 & a_1b_1 & c_1^2 \\ a_2^3c_2 & a_2b_2 & c_2^2 \\ a_3^3c_3 & a_3b_3 & c_3^2\end{vmatrix} + \begin{vmatrix} a_1^4 & a_1^3c_1 & c_1^2 \\ a_2^4 & a_2^3c_2 & c_2^2 \\ a_3^4 & a_3^3c_3 & c_3^2\end{vmatrix}\right\}\cdot\Lambda,
\end{aligned}
\tag{16}
$$

and

$$
\Lambda = \Lambda_5\alpha^5 + \Lambda_4\alpha^4 + \Lambda_3\alpha^3 + \Lambda_2\alpha^2 + \Lambda_1\alpha + \Lambda_0,
\tag{17}
$$

with

$$
\begin{aligned}
\Lambda_5 = {}& \frac{b_2^2b_3^2[(3a_2b_3 - a_3b_2)a_3c_2 + a_2c_3(a_2b_3 - 3a_3b_2)]}{2}c_1^4 \\
&- \frac{3b_1b_2b_3(a_2b_3 - a_3b_2)(a_2b_2c_3^2 + a_3b_3c_2^2)}{2}c_1^3 \\
&- \frac{3b_1b_2b_3(a_2b_2c_3^2 + a_3b_3c_2^2)[(a_3b_1 - a_1b_3)c_2 + c_3(a_1b_2 - a_2b_1)]}{2}c_1^2 \\
&+ \frac{3}{2}b_1^2(a_2b_2c_3^2 + a_3b_3c_2^2)\left[(-a_1b_3 + \frac{1}{3}a_3b_1)b_3c_2^2 + c_3^2b_2(a_1b_2 - \frac{1}{3}a_2b_1)\right]c_1 \\
&+ \frac{a_1b_1^2c_2c_3(b_2c_3 - b_3c_2)}{2} \\
&\times [(a_1b_3 - 3a_3b_1)b_3c_2^2 - 2a_1b_2b_3c_3c_2 + c_3^2b_2(a_1b_2 - 3a_2b_1)],
\end{aligned}
\tag{18}
$$

$$
\begin{aligned}
\Lambda_4 = {}& b_2b_3(3a_2^4b_3^2 + 3a_2a_3^3b_2b_3 - a_3^4b_2^2)(a_3c_2 - a_2c_3)c_1^4 - \frac{3}{2}(a_2b_3 - a_3b_2) \\
&\times [(a_1^3b_2b_3 + 2a_3^3b_1b_2 + a_2^3b_1b_3)a_3b_3c_2^2 + (a_1^3b_2b_3 + 2a_2^3b_1b_3 + a_3^3b_1b_2) \\
&\times a_2b_2c_3^2]c_1^3 - \frac{3}{2}c_1^2[(a_1b_2 - a_2b_1)c_3 - (a_1b_3 - a_3b_1)c_2] \\
&\times [(a_1^3b_2b_3 + a_2^3b_1b_3 + 2a_3^3b_1b_2)a_3b_3c_2^2 + (a_1^3b_2b_3 + a_3^3b_1b_2 + 2a_2^3b_1b_3)a_2b_2c_3^2] \\
&+ 3b_1\left[a_2b_2c_3^4(a_1^4b_2^2 + a_1a_2^3b_1b_2 - \frac{1}{3}a_2^4b_1^2) - a_3b_3c_2^4(a_1^4b_3^2 + a_1a_3^3b_1b_3\right. \\
&\left.- \frac{1}{3}a_3^4b_1^2) - a_1c_2^2c_3^2(a_2b_3 - a_3b_2)\left(a_1^3b_2b_3 + \frac{b_1(a_2^3b_3 + a_3^3b_2)}{2}\right)\right]c_1 \\
&+ a_1b_1c_2c_3\left\{b_2c_3^3(a_1^4b_2^2 - 3a_1^3a_2b_1b_2 - 3a_2^4b_1^2)\right. \\
&+ 3\left(a_1^3b_2b_3 + \frac{b_1(a_2^3b_3 + a_3^3b_2)}{2}\right)[(a_1b_3 - a_3b_1)c_3c_2^2 - (a_1b_2 - a_2b_1)c_2c_3^2] \\
&\left.- b_3c_2^3(a_1^4b_3^2 - 3a_1^3a_3b_1b_3 - 3a_3^4b_1^2)\right\},
\end{aligned}
\tag{19}
$$

$$
\begin{aligned}
\Lambda_3 =& \bigg\{\frac{3}{2}a_3c_2\bigg(a_2^7b_3^3 + a_2^6a_3b_2b_3^2 + 4a_2^4a_3^3b_2b_3^2 + a_2a_3^6b_2^2b_3 - \frac{1}{3}a_3^7b_2^3\bigg)\\
&+ \frac{3}{2}a_2c_3\bigg(\frac{1}{3}a_2^7b_3^3 - a_2^6a_3b_2b_3^2 - 4a_2^3a_3^4b_2^2b_3 - a_2a_3^6b_2^2b_3 - a_3^7b_2^3\bigg)\bigg\}c_1^4\\
&- 3(a_2b_3 - a_3b_2)\bigg\{\frac{1}{2}a_3c_2^2(a_1^3(a_2^3b_3^2 + 2a_3^3b_2b_3) + a_3^3(a_3^3b_1b_2 + 2a_2^3b_1b_3))\\
&+ a_2c_3^2\bigg(a_1^3b_2\bigg(a_2^3b_3 + \frac{a_3^3b_2}{2}\bigg) + a_2^3b_1\bigg(\frac{a_2^3b_3}{2} + a_3^3b_2\bigg)\bigg)\bigg\}c_1^3\\
&- [3(c_3(a_1b_2 - a_2b_1) - c_2(a_1b_3 + a_3b_1))]c_1^2\bigg\{\frac{1}{2}a_3c_2^2(a_1^3(a_2^3b_3^2 + 2a_3^3b_2b_3)\\
&+ a_3^3(a_3^3b_1b_2 + 2a_2^3b_1b_3)) + a_2c_3^2\bigg[a_1^3b_2\bigg(a_2^3b_3 + \frac{a_3^3b_2}{2}\bigg) + a_2^3b_1\bigg(\frac{a_2^3b_3}{2} + a_3^3b_2\bigg)\bigg]\bigg\}\\
&+ \bigg\{\frac{3}{2}a_2c_3^4\bigg(a_1^7b_2^3 + a_1^6a_2b_1b_2^2 + 4a_1^4a_2^3b_1b_2^2 + a_1a_2^6b_1^2b_2 - \frac{1}{3}a_2^7b_1^3\bigg)\\
&- \frac{3}{2}a_3c_2^4\bigg(a_1^7b_3^3 + a_1^6a_3b_1b_3^2 + 4a_1^4a_3^3b_1b_3^2 + a_1a_3^6b_1^2b_3 - \frac{1}{3}a_3^7b_1^3\bigg)\\
&- \frac{3}{2}a_1c_2^2c_3^2(a_2b_3 - a_3b_2)\big[a_1^6b_2b_3 + 2a_1^3b_1(a_2^3b_3 + a_3^3b_2) + a_2^3a_3^3b_1^2\big]\bigg\}c_1\\
&+ \frac{1}{2}a_1c_2c_3\big\{c_3^3(a_1^7b_2^3 - 3a_1^6a_2b_1b_2^2 - 12a_1^3a_2^4b_1^2b_2 - 3a_1a_2^6b_1^2b_2 - 3a_2^7b_1^3)\\
&- c_2^3(a_1^7b_3^3 - 3a_1^6a_3b_1b_3^2 - 12a_1^3a_3^4b_1^2b_3 - 3a_1a_3^6b_1^2b_3 - 3a_3^7b_1^3)\\
&+ \big[3c_2^2c_3(a_1b_3 - a_3b_1) - 3c_2c_3^2(a_1b_2 - a_2b_1)\big]\\
&\times \big[a_1^6b_2b_3 + 2a_1^3b_1(a_2^3b_3 + a_3^3b_2) + a_2^3a_3^3b_1^2\big]\big\},
\end{aligned}
\tag{20}
$$

$$
\begin{aligned}
\Lambda_2 =& a_2^2a_3^2\bigg(3a_2^2b_3c_2\bigg(a_2^3a_3^2b_3 + a_2^2a_3^3b_2 + a_3^5b_2 + \frac{1}{3}a_2^5b_3\bigg) - a_3^2b_2c_3\\
&\times\bigg(a_2^3a_3^2b_3 + a_2^2a_3^3b_2 + a_2^5b_3 + \frac{1}{3}a_3^5b_2\bigg)\bigg)c_1^4 - \frac{3}{2}c_1^3(a_2b_3 - a_3b_2)\\
&\times \big[a_3^4c_2^2\big((2a_2^3b_3 + a_3^3b_2)a_1^3 + a_2^3a_3^3b_1\big) + a_2^4c_3^2\big((a_2^3b_3 + 2a_3^3b_2)a_1^3 + a_2^3a_3^3b_1\big)\big]\\
&- \frac{3}{2}[c_3(a_1b_2 - a_2b_1) - c_2(a_1b_3 - a_3b_1)]\big[a_3^4c_2^2((2a_2^3b_3 + a_3^3b_2)a_1^3\\
&+ a_2^3a_3^3b_1) + a_2^4c_3^2((a_2^3b_3 + 2a_3^3b_2)a_1^3 + a_2^3a_3^3b_1)\big]c_1^2 + \Big[a_2^2b_2c_3^4\\
&\times (a_1^5b_2 + 3a_1^3a_2^2b_2 + 3a_1^2a_2^3b_1 + 3a_2^5b_1) - a_3^2b_3c_2^4(a_1^5b_3 + 3a_1^3a_3^2b_3\\
&+ 3a_1^2a_3^3b_1 + 3a_3^5b_1) - \frac{3}{2}c_2^2c_3^2(a_2b_3 - a_3b_2)\big((a_2^3b_3 + a_3^3b_2)a_1^3 + 2a_2^3a_3^3b_1\big)\Big]c_1\\
&- \frac{3}{2}a_1^2c_2c_3\bigg[2a_2^4b_1c_3^3(a_1^5b_2 + a_2^2b_2a_1^3 + a_2^3b_1a_1^2 + \frac{1}{3}b_1a_2^5)
\end{aligned}
$$

$$- 2a_3^4b_1c_2^3\left(a_1^5b_3 + a_3^2b_3a_1^3 + a_3^3b_1a_1^2 + \frac{1}{3}b_1a_3^5\right) + a_1^2c_2c_3^2(a_1b_2 - a_2b_1)((a_2^3b_3 + a_3^3b_2)a_1^3 + 2a_2^3a_3^3b_1) - a_1^2c_2^2c_3(a_1b_3 - a_3b_1)((a_2^3b_3 + a_3^3b_2)a_1^3 + 2a_2^3a_3^3b_1)\Bigg], \tag{21}$$

$$\begin{aligned}\Lambda_1 = {} & \left(a_2c_2\left(a_2^3b_3 + \frac{3}{4}a_2a_3^2b_3 + \frac{3}{4}a_3^3b_2\right) - a_3c_3\left(\frac{3}{4}a_2^3b_3 + \frac{3}{4}a_2^2a_3b_2 + a_3^3b_2\right)\right) \\ & \times\ 2a_2^5a_3^5c_1^4 - \frac{3}{2}a_1^3a_2^3a_3^3(a_2^4c_3^2 + a_3^4c_2^2)(a_2b_3 - a_3b_2)c_1^3 - \frac{3}{2}a_1^3a_2^3a_3^3(a_2^4c_3^2 + a_3^4c_2^2) \\ & \times\ [c_3(a_1b_2 - a_2b_1) - c_2(a_1b_3 - a_3b_1)]c_1^2 + \Bigg(a_2^5c_3^4(a_1^3b_2 + \frac{3}{4}a_1a_2^2b_2 + \frac{3}{4}a_2^3b_1) \\ & - a_3^5c_2^4(a_1^3b_3 + \frac{3}{4}a_1a_3^2b_3 + \frac{3}{4}a_3^3b_1) - \frac{3}{4}a_1a_2^3a_3^3c_2^2c_3^2(a_2b_3 - a_3b_2)\Bigg)2a_1^6c_1 \\ & - \frac{3}{2}a_1^5c_2c_3\Bigg[a_2^6c_3^3(a_1^3b_2 + a_1^2a_2b_1 + \frac{4}{3}a_2^3b_1) - a_3^6c_2^3(a_1^3b_3 + a_1^2a_3b_1 + \frac{4}{3}a_3^3b_1) \\ & + a_1^2a_2^3a_3^3c_2c_3^2(a_1b_2 - a_2b_1) - a_1^2a_2^3a_3^3c_2^2c_3(a_1b_3 - a_3b_1)\Bigg],\end{aligned} \tag{22}$$

$$\Lambda_0 = a_2^8a_3^8c_1^4(a_2c_2 - a_3c_3) + (a_2^8c_3^4 - a_3^8c_2^4)a_1^9c_1 + a_1^8(a_3^9c_2^4c_3 - a_2^9c_2c_3^4), \tag{23}$$

where $S = \{(1,1,1),(1,1,-1),(1,-1,1),(-1,1,1)\}$. Given that the final term does not inherently equate to zero, the $(3+1)$-dimensional bilinear HSI equation (10) lacks three-soliton solutions. This absence of three-soliton solutions further suggests that the $(3+1)$-dimensional HSI equation (8) is non-integrable. Nonetheless, from (16), it is evident that under specific conditions, the function f as defined in (25) can yield three-soliton solutions:

- One of the three wave numbers a_1, a_2, a_3 is zero;
- The constants a_i, b_i, and c_i satisfy the following equation:

$$\alpha^2\begin{vmatrix} a_1b_1 & b_1c_1 & c_1^2 \\ a_2b_2 & b_2c_2 & c_2^2 \\ a_2b_3 & b_3c_3 & c_3^2 \end{vmatrix} + \alpha\begin{vmatrix} a_1^4 & b_1c_1 & c_1^2 \\ a_2^4 & b_2c_2 & c_2^2 \\ a_3^4 & b_2c_3 & c_3^2 \end{vmatrix} - \alpha\begin{vmatrix} a_1^3c_1 & a_1b_1 & c_1^2 \\ a_2^3c_2 & a_2b_2 & c_2^2 \\ a_3^3c_3 & a_3b_3 & c_3^2 \end{vmatrix} + \begin{vmatrix} a_1^4 & a_1^3c_1 & c_1^2 \\ a_2^4 & a_2^3c_2 & c_2^2 \\ a_3^4 & a_3^3c_3 & c_3^2 \end{vmatrix} = 0. \tag{24}$$

It is crucial to note that $a_i^3 \neq -\alpha b_i$. In this study, our primary focus will be on applying the second condition.

2.2. *Multi-soliton solutions*

Based on Hirota's bilinear method, the N-soliton solution of Eq. (8) is

$$f = \sum_{\mu=0,1} \exp\left(\sum_{s=1}^{N} \mu_s\eta_s + \sum_{s<j} a_{sj}\mu_s\mu_j\right), \tag{25}$$

where $\mu = 0, 1$ means that each μ_s takes 0 or 1, and

$$\eta_s = a_s x + b_s y + c_s z + d_s t + \eta_s^0, \quad d_s = -\frac{\beta c_s^2}{a_s^3 + \alpha b_s}, \quad 1 \le s \le N, \tag{26}$$

$$\begin{aligned} \mathrm{e}^{a_{sj}} &= A_{sj} \\ &= \frac{l_{sj}^2 + 3(a_j^3 c_s^2 - \alpha(b_s c_j^2 - b_j c_s^2))(a_s^2 a_j - a_s a_j^3) + 3a_s^4 a_j c_j^2 (a_j - a_s)}{l_{sj}^2 + 3(a_j^3 c_s^2 + \alpha(b_s c_j^2 + b_j c_s^2))(a_s^2 a_j + a_s a_j^3) + 3a_s^4 a_j c_j^2 (a_j + a_s)}, \\ &\qquad 1 \le s < j \le N, \end{aligned} \tag{27}$$

and

$$l_{sj} = a_j^3 c_s - a_s^3 c_j - \alpha(b_s c_j - b_j c_s), \tag{28}$$

where $a_s, b_s, c_s, d_s, \eta_s^0$ are constants. The constants a_s, b_s, c_s need to satisfy the condition (24) for $N \ge 3$.

3. Soliton-Type Solutions

This section is dedicated to the exploration of *N*-soliton solutions for the $(3+1)$-dimensional HSI equation (8), building upon the three-soliton conditions delineated in Sec. 2. The discussion encompasses a comprehensive analysis of soliton, breather, and lump solutions, as well as their interaction solutions, for $N = 1, 2, 3, 4$.

3.1. *Soliton solution*

In the context of the one-soliton solution $(N = 1)$ for the HSI equation (8), the initial step involves scrutinizing Eq. (25) to ascertain an expression for the function *f*, which is formulated as follows:

$$f = 1 + \exp(\eta_1). \tag{29}$$

The derivation of the one-soliton solution for the HSI equation (8) entails substituting the expression from Eq. (29) into the bilinear transformation provided by Eq. (9). This substitution results in the following expressions for the components within the soliton solution:

$$\begin{aligned} u &= \frac{a_1^2}{2}\operatorname{sech}^2\left(\frac{1}{2}\eta_1\right), \\ p &= \frac{a_1 b_1}{2}\operatorname{sech}^2\left(\frac{1}{2}\eta_1\right), \\ w &= -\frac{a_1}{4}\frac{\beta c_1^2}{a_1^3 + \alpha b_1}\operatorname{sech}^2\left(\frac{1}{2}\eta_1\right), \\ q &= \frac{a_1 c_1}{2}\operatorname{sech}^2\left(\frac{1}{2}\eta_1\right), \end{aligned} \tag{30}$$

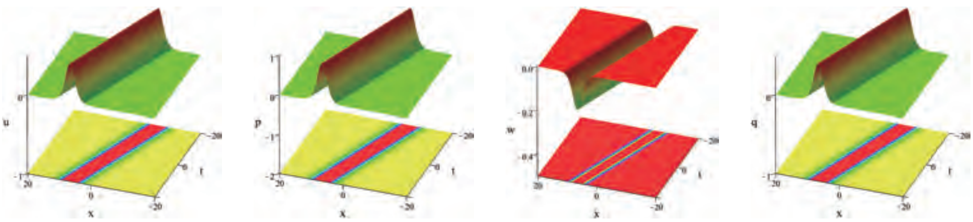

(a) (b) (c) (d)

Fig. 1. (Color online) One-soliton solution (30) with $\alpha = 1$, $\beta = 1$, $a_1 = 1$, $b_1 = 2$, $c_1 = 1$, and $\eta_1^0 = 0$.

where $\eta_1 = a_1 x + b_1 y + c_1 z - \frac{\beta c_1^2}{a_1^3 + \alpha b_1} t + \eta_1^0$. The behavior of these soliton components can be observed by examining different parameters. Specifically, setting $a_1 = 1$, $b_1 = 2$, and $c_1 = 1$, it is ensured that u, p, and q are all positive. On the other hand, the sign of the component w depends on the parameters α and β. For example, when taking $\alpha = 1$, $\beta = 1$, and $\eta_1^0 = 0$ at $z = 0$ and $y = 0$, the soliton solution exhibits interesting features. In Fig. 1, components u, p, and q exhibit a bell-shaped soliton profile, while the component w shows an anti-bell-shaped soliton profile. Apart from the visual characteristics, several physical quantities can be derived from solutions (30). Notably, the amplitudes of the solutions u, p, w, and q can be determined as $\frac{a_1^2}{2}$, $\frac{a_1 b_1}{2}$, $-\frac{a_1}{4}\frac{\beta c_1^2}{a_1^3 + \alpha b_1}$, and $\frac{a_1 c_1}{2}$, respectively. Additionally, the envelope velocities along the x-axis, y-axis, and z-axis are given by $\frac{\beta c_1^2}{a_1^4 + \alpha a_1 b_1}$, $\frac{\beta c_1}{a_1^3 b_1 + \alpha b_1^2}$, and $\frac{\beta c_1^2}{a_1^3 + \alpha b_1}$, respectively.

In Eq. (25), the two-soliton solution for $N = 2$ is expressed as follows:

$$f = 1 + \exp(\eta_1) + \exp(\eta_2) + A_{12} \exp(\eta_1 + \eta_2), \tag{31}$$

where η_1, η_2, and A_{12} are defined in accordance with (26) and (27), respectively. Given the assurance of the presence of two solitons, the parameters can be arbitrarily selected. Upon substituting Eq. (31) into Eq. (9), the resultant figure of the two-soliton solution is depicted in Fig. 2(a).

When $N = 3$, the three-soliton solution from Eq. (25) is expressed as follows:

$$f = 1 + \sum_{s=1}^{3} \exp(\eta_s) + \sum_{s<j}^{3} A_{sj} \exp(\eta_s + \eta_j) + A_{123} \exp(\eta_1 + \eta_2 + \eta_3), \tag{32}$$

where η_s $(s = 1, 2, 3)$ and A_{ij} are defined as (26) and (27), respectively, and $A_{123} = A_{12} A_{13} A_{23}$. At this point, we need to consider the parameters satisfying the condition for the existence of three solitons, that is, (a_1, a_2, a_3) and (c_1, c_2, c_3) are parallel. The plot of the three-soliton solution for Eq. (8) can be obtained by substituting Eq. (32) into Eq. (9), as depicted in Fig. 2(b).

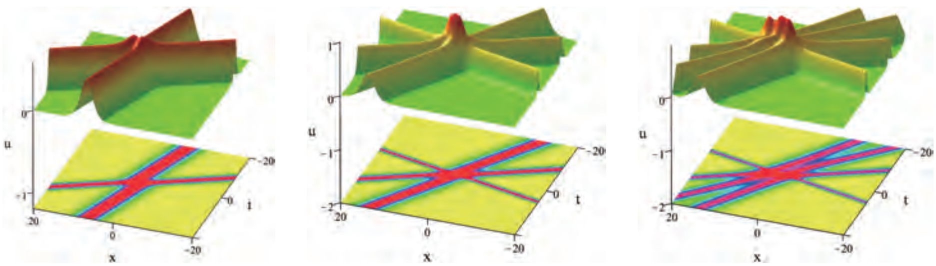

(a) (b) (c)

Fig. 2. (Color online) Soliton solutions from (31)–(33) and (9): (a) two-soliton solution with $\alpha = 1$, $\beta = 1$, $a_1 = 1$, $b_1 = 1$, $c_1 = 2$, $a_2 = 1$, $b_2 = 2$, $c_2 = 1$, $\eta_1^0 = \eta_2^0 = 0$; (b) three-soliton solution with $\alpha = 1$, $\beta = 1$, $a_1 = 1$, $b_1 = 1$, $c_1 = 2$, $a_2 = 1$, $b_2 = 5$, $c_2 = 2$, $a_3 = 1$, $b_3 = -2$, $c_3 = 2$, $\eta_1^0 = \eta_2^0 = \eta_3^0 = 0$; (c) four-soliton solution with $\alpha = 1$, $\beta = 1$, $a_1 = 1$, $b_1 = 1$, $c_1 = 2$, $a_2 = 1$, $b_2 = 5$, $c_2 = 2$, $a_3 = 1$, $b_3 = -2$, $c_3 = 2$, $a_4 = 1$, $b_4 = 3$, $c_4 = 2$, $\eta_1^0 = \eta_2^0 = \eta_3^0 = \eta_4^0 = 0$.

For $N = 4$, the four-soliton solution arising from Eq. (25) is given by

$$\begin{aligned} f = 1 &+ \sum_{s=1}^{4} \exp(\eta_s) + \sum_{s<j}^{4} A_{sj} \exp(\eta_s + \eta_j) \\ &+ \sum_{s<j<k} A_{sjk} \exp(\eta_s + \eta_j + \eta_k) + A_{1234} \exp\left(\sum_{s=1}^{4} \eta_s\right), \end{aligned} \tag{33}$$

where η_s $(s = 1, 2, 3, 4)$ and A_{ij} are defined as (26) and (27), respectively, and $A_{1234} = A_{12}A_{13}A_{14}A_{23}A_{24}A_{34}$. The conditions for the existence of four solitons can be referenced from the conditions for three solitons, represented as (a_1, a_2, a_3, a_4) and (c_1, c_2, c_3, c_4). Upon substituting Eq. (33) into Eq. (9), the graphical representation of the four-soliton solution for Eq. (9) is obtained, as depicted in Fig. 2(c). The components u, p, w, q of the two-soliton to four-soliton solution are similar to the one-soliton solution, thus only the plot of the component u is presented in Fig. 2.

3.2. *Breather solution*

Employing the complex conjugate parameter method, breather solutions across various planes can be derived from the soliton solutions. If setting $a_1 = a_2^* = \nu_{1R} + \mathrm{I}\nu_{1I}$, $b_1 = b_2 = \omega_1$, $c_1 = c_2^* = \nu_{1R} + \mathrm{I}\nu_{1I}$, $\eta_1^0 = \eta_2^0 = 0$, where I stands for the imaginary unit, i.e. $\mathrm{I}^2 = -1$, the function in (31) is

$$f = 1 + A_{12}e^{2\zeta_1} + 2e^{\zeta_1}\cos\vartheta_1, \tag{34}$$

with

$$\begin{aligned} A_{12} = (&[\nu_{1I}(\omega_1 + \omega_2) - \nu_{1R}(\omega_1 - \omega_2)]^2\alpha^2 + 4\nu_{1I}^2(\nu_{1R}^2 - 3\nu_{1I}^2)(\nu_{1R}^2 + \nu_{1I}^2)^2 \\ &- 2\alpha\nu_{1I}(\nu_{1R}^2 + \nu_{1I}^2)[\mathrm{I}(\omega_1 - \omega_2)(\nu_{1R}^2 + 3\nu_{1I}^2) - 2\nu_{1R}\nu_{1I}(\omega_1 + \omega_2)])/ \end{aligned}$$

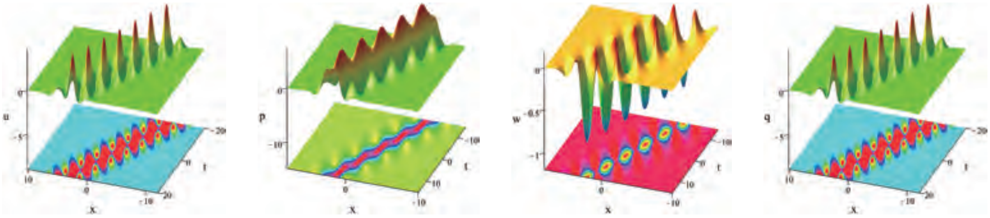

(a) (b) (c) (d)

Fig. 3. (Color online) One-breather solutions from (34) and (9) in (x,t)-plane with $\alpha=1$, $\beta=1$, $\nu_{1R}=1$, $\nu_{1I}=2$, $\omega_1=3$.

$$\times\ ([\nu_{1I}(\omega_1+\omega_2)-\nu_{1R}(\omega_1-\omega_2)]^2\alpha^2-12\nu_{1R}^2(\nu_{1R}^2-\frac{1}{3}\nu_{1I}^2)(\nu_{1R}^2+\nu_{1I}^2)^2$$
$$+\ 4\alpha\nu_{1R}(\nu_{1R}^2+\nu_{1I}^2)[(\mathrm{I}\nu_{1I}\nu_{1R}-\frac{3}{2}\nu_{1R}^2)(\omega_1-\omega_2)-\frac{1}{2}\nu_{1I}^2(\omega_1+\omega_2)]), \tag{35}$$

$$\zeta_1=\nu_{1R}x+\omega_1 y+\nu_{1R}z+\left(-\frac{\beta(\nu_{1R}^2-\nu_{1I}^2)(\nu_{1R}^3-3\nu_{1R}\nu_{1I}^2+\alpha\omega_1)}{(\nu_{1R}^3-3\nu_{1R}\nu_{1I}^2+\alpha\omega_1)^2+(3\nu_{1R}^2\nu_{1I}-\nu_{1I}^3)^2}\right.$$
$$\left.-\frac{2\beta\nu_{1R}\nu_{1I}(3\nu_{1R}^2\nu_{1I}-\nu_{1I}^3)}{(\nu_{1R}^3-3\nu_{1R}\nu_{1I}^2+\alpha\omega_1)^2+(3\nu_{1R}^2\nu_{1I}-\nu_{1I}^3)^2}\right)t, \tag{36}$$

$$\vartheta_1=\nu_{1I}x+\nu_{1I}z+\left(-\frac{2\beta\nu_{1R}\nu_{1I}(\nu_{1R}^3-3\nu_{1R}\nu_{1I}^2+\alpha\omega_1)}{(\nu_{1R}^3-3\nu_{1R}\nu_{1I}^2+\alpha\omega_1)^2+(3\nu_{1R}^2\nu_{1I}-\nu_{1I}^3)^2}\right.$$
$$\left.-\frac{\beta(\nu_{1R}^2-\nu_{1I}^2)(3\nu_{1R}^2\nu_{1I}-\nu_{1I}^3)}{(\nu_{1R}^3-3\nu_{1R}\nu_{1I}^2+\alpha\omega_1)^2+(3\nu_{1R}^2\nu_{1I}-\nu_{1I}^3)^2}\right)t. \tag{37}$$

In the (x,t)-plane (see Fig. 3), when $\nu_{1R}=1$, $\nu_{1I}=2$, $\omega_1=3$, the solutions u, p, w, q form shapes that exhibit a breather motion. This movement remains continuous and stable on other planes, with shapes staying unchanged during propagation. However, in the (x,z)-plane, at the same parameter values, the shapes of these solutions undergo noticeable changes, as shown in Fig. 4(a). Conversely, when ν_{1R} is set to 0

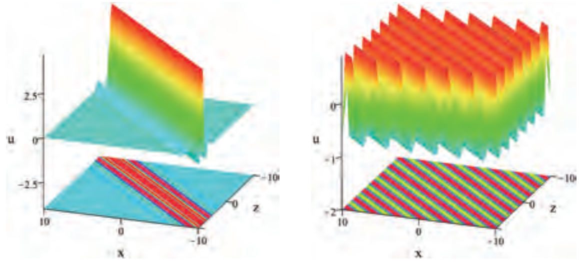

(a) (b)

Fig. 4. (Color online) Periodic solutions (34) and (9) in (x,z)-plane with $\alpha=1$, $\beta=1$, $\nu_{1I}=2$, $\omega_1=3$, (a) $\nu_{1R}=1$; (b) $\nu_{1R}=0$.

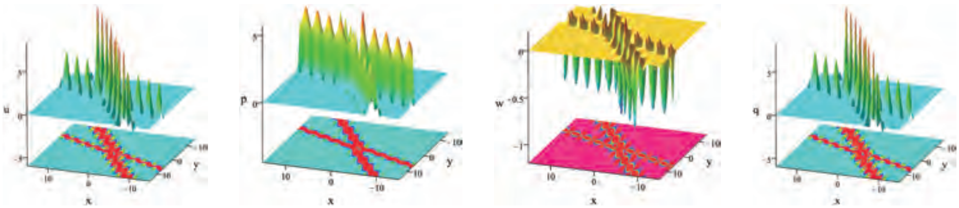

(a) (b) (c) (d)

Fig. 5. (Color online) Two-breather solutions from (38) and (9) in (x,y)-plane with $\alpha=1$, $\beta=1$, $\nu_{1R}=1$, $\nu_{2R}=\frac{3}{2}$, $\nu_{1I}=2$, $\nu_{2I}=\frac{5}{2}$, $\omega_1=2$, $\omega_2=1$.

while keeping $\nu_{1I}=2$ and $\omega_1=3$ constant, the shape in Fig. 4(a) transitions into a periodic solution, as depicted in Fig. 4(b). This transformation highlights the influence of the parameter ν_{1R} on the morphological and dynamic characteristics of solution sets across different planes, emphasizing its significance in system behavior.

By setting $a_1=a_2^*=\nu_{1R}+\mathrm{I}\nu_{1I}$, $a_3=a_4^*=\nu_{2R}+\mathrm{I}\nu_{2I}$, $b_1=b_2=\omega_1$, $b_3=b_4=\omega_2$, $c_1=c_2^*=\nu_{1R}+\mathrm{I}\nu_{1I}$, $c_3=c_4^*=\nu_{2R}+\mathrm{I}\nu_{2I}$, and $\eta_1^0=\eta_2^0=\eta_3^0=\eta_4^0=0$, while satisfying the Hirota bilinear condition, the function in (33) can be expressed as follows:

$$
\begin{aligned}
f =\,& 1 + A_{12}\mathrm{exp}\,(2\zeta_1) + A_{34}\mathrm{exp}\,(2\zeta_2) + 2\mathrm{exp}\,(\zeta_1)\cos\vartheta_1 + 2\mathrm{exp}\,(\zeta_2)\cos\vartheta_2\\
&+ 2M_3\mathrm{exp}\,(\zeta_1+\zeta_2)\cos(\vartheta_1+\vartheta_2+\omega_3) + 2M_4\mathrm{exp}\,(\zeta_1+\zeta_2)\cos(\vartheta_1-\vartheta_2-\omega_4)\\
&+ 2A_{12}M_3M_4\mathrm{exp}\,(2\zeta_1+\xi_2)\cos(\vartheta_2+\omega_3+\omega_4) + 2A_{34}M_3M_4\mathrm{exp}\,(\zeta_1+2\zeta_2)\\
&\times\cos(\vartheta_1+\omega_3-\omega_4) + A_{12}A_{34}M_3^2M_4^2\mathrm{exp}\,(2\zeta_1+2\zeta_2),
\end{aligned}
\tag{38}
$$

with

$$
\begin{aligned}
A_{13} &= M_3\mathrm{exp}\,(\mathrm{I}\omega_3) = A_{24}^*,\\
A_{14} &= M_4\mathrm{exp}\,(-\mathrm{I}\omega_4) = A_{23}^*.
\end{aligned}
\tag{39}
$$

Furthermore, when $\nu_{1R}=1$, $\nu_{1I}=2$, $\omega_1=2$, $\nu_{2R}=\frac{3}{2}$, $\nu_{2I}=\frac{5}{2}$, $\omega_2=1$, the resulting solutions u, p, w, q form shapes that exhibit a two-breather motion, as shown in Fig. 5.

3.3. *Lump solution*

In the realm of mathematical methods, the long-wave limit stands as a powerful tool, particularly adept at approximating systems where wave wavelengths significantly surpass the system's dimensions. A prime application lies in the study of fluid dynamics, such as water waves, where wavelengths dwarf the depth of the medium.[22]

This section delves into harnessing the long-wave limit method to derive lump solutions from the N-soliton solutions of Eq. (8). Through the assignment of, $a_i=l_i\varepsilon$, $b_i=m_ia_i$, $c_i=n_ia_i$ and $\eta_i^0=\mathrm{I}\pi$, a reformulation of Eq. (31) emerges

$$
f = l_1l_2\varepsilon^2(\chi_1\chi_2+\varpi_{12}) + o(\varepsilon^3),
\tag{40}
$$

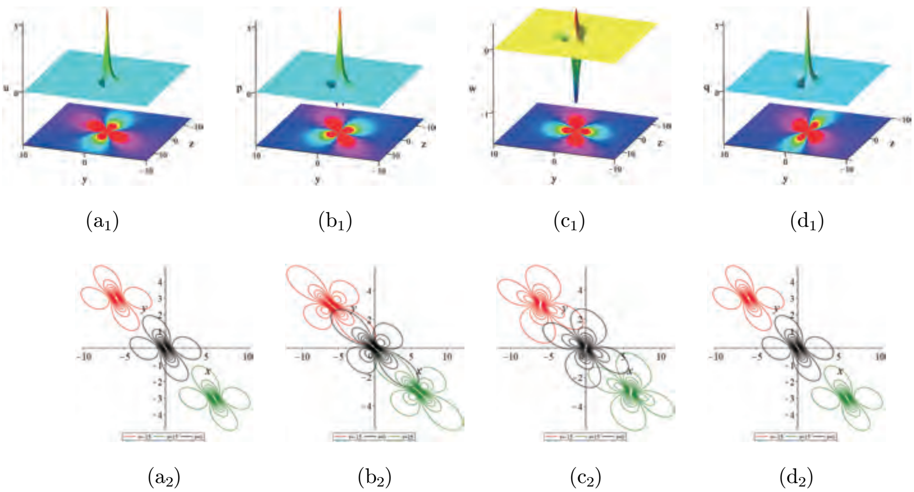

Fig. 6. (Color online) One-lump solution from (40) and (9) in (y, z)-plane, with a 3D (top) and density (bottom) plots in the upper layer (a$_1$)–(d$_1$), and the corresponding time evolution contour plot at different times below (a$_2$)–(d$_2$).

where

$$\chi_i = x + m_i y + n_i z - \frac{\beta n_i^2}{a_i^2 + \alpha m_i} t, \varpi_{12} = -\frac{6(m_1 n_2^2 + m_2 n_1^2)}{\alpha(m_1 n_2 - m_2 n_1)^2}, \quad i = 1, 2. \tag{41}$$

By substituting Eq. (40) into Eq. (9), and taking the limit as $\varepsilon \to 0$, the solutions of Eq. (8) can be expressed as follows:

$$\begin{aligned} u &= \frac{4}{\chi_1\chi_2 + \chi_0} - \frac{2(\chi_1 + \chi_2)^2}{(\chi_1\chi_2 + \chi_0)^2}, \\ p &= \frac{2(m_1 + m_2)}{\chi_1\chi_2 + \chi_0} - \frac{2(\chi_1 + \chi_2)(m_1\chi_2 + m_2\chi_1)}{(\chi_1\chi_2 + \chi_0)^2}, \\ w &= -\frac{2\beta\left(\frac{n_1^2}{\alpha m_1} + \frac{n_2^2}{\alpha m_2}\right)}{\chi_1\chi_2 + \chi_0} - \frac{2(\chi_1 + \chi_2)\left(-\frac{\beta n_1^2}{\alpha m_1}\chi_2 - \frac{\beta n_2^2}{\alpha m_2}\chi_1\right)}{(\chi_1\chi_2 + \chi_0)^2}, \\ q &= \frac{2(n_1 + n_2)}{\chi_1\chi_2 + \chi_0} - \frac{2(\chi_1 + \chi_2)(n_1\chi_2 + n_2\chi_1)}{(\chi_1\chi_2 + \chi_0)^2}. \end{aligned} \tag{42}$$

Moreover, with the parameters $\alpha = 1$, $\beta = 1$, $a_1 = 1$, $a_2 = 5$, $m_1 = m_2^* = 1 + 2\mathrm{I}$, $n_1 = n_2^* = 1$, it is observed that the two-soliton solution will degenerate into one lump u, p, w, q as shown in Fig. 6 in (y, z)-plane. After computation, it is determined that $u_{\max}(\frac{2t}{5} - z, -\frac{t}{5}, z) = \frac{16}{3}$ and $u_{\min}(\frac{2t}{5} - z + \frac{3}{2}, -\frac{t}{5}, z) = u_{\min}\,(\frac{2t}{5} - z - \frac{3}{2}, -\frac{t}{5}, z) = -\frac{2}{3}$. Hence, the amplitude of one lump is 6. The time evolution plots in Fig. 6 (a$_2$)–(d$_2$) at $t = -15, t = 0$ and $t = 15$ depict the dynamics of the four components u, p, w, and q. As they progress along the line defined by

$$y = -\frac{a_1^2 c_2^2 - a_2^2 c_1^2 + \alpha(b_1 c_2^2 - b_2 c_1^2)}{a_1^2 b_1 c_2^2 - a_2^2 b_2 c_1^2 + \alpha(b_1^2 c_2^2 - b_2^2 c_1^2)}, \tag{43}$$

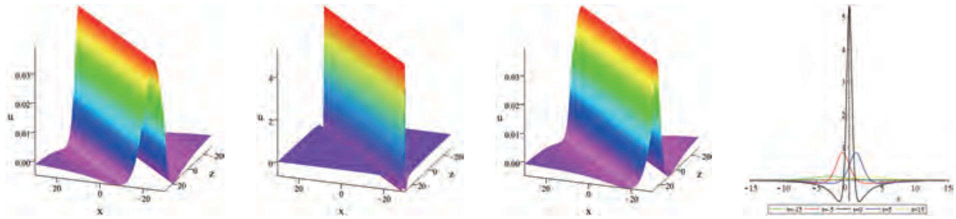

(a) (b) (c) (d)

Fig. 7. (Color online) The time evolution of the one-line lump solution from (40) and (9) in the (x,z)-plane.

which simplifies to

$$y = \left(-\frac{17}{18} - \frac{28}{87}\right)x, \tag{44}$$

they undergo a shift. However, within the (x,z)-plane, it transforms into a line-lump, gradually appearing and disappearing over time, as depicted in Figs. 7(a)–7(d), which provides a more intuitive visualization.

The parameters under the Hirota N-soliton condition are initially redefined as $a_i = l_i\varepsilon$, $b_i = m_i a_i$, $c_i = n_i a_i$, and $\eta_i^0 = \mathrm{I}\pi$ for $i = 1,2,3,4$, with $\varepsilon \to 0$. In the pursuit of capturing the essence of the system's evolution, the expression for f provided in Eq. (33) as follows:

$$\begin{aligned} f = (&\chi_1\chi_2\chi_3\chi_4 + \varpi_{34}\chi_1\chi_2 + \varpi_{24}\chi_1\chi_3 + \varpi_{23}\chi_1\chi_4 + \varpi_{14}\chi_2\chi_3 + \varpi_{13}\chi_2\chi_4 \\ &+ \varpi_{12}\chi_3\chi_4 + \varpi_{12}\varpi_{34} + \varpi_{13}\varpi_{24} + \varpi_{14}\varpi_{23})l_1l_2l_3l_4\varepsilon^4 + o(\varepsilon^4). \end{aligned} \tag{45}$$

By fixing $\alpha = 1$, $\beta = 1$, $a_1 = 1$, $a_2 = 5$, $m_1 = m_2^* = 1 + 2\mathrm{I}$, and $n_1 = n_2^* = 1$, the resultant two-lump solution u can be visually depicted in Fig. 8. This visualization elegantly captures the evolving dynamics of the two-lump configuration within the (x,y)-plane as time progresses, akin to an elastic collision scenario.

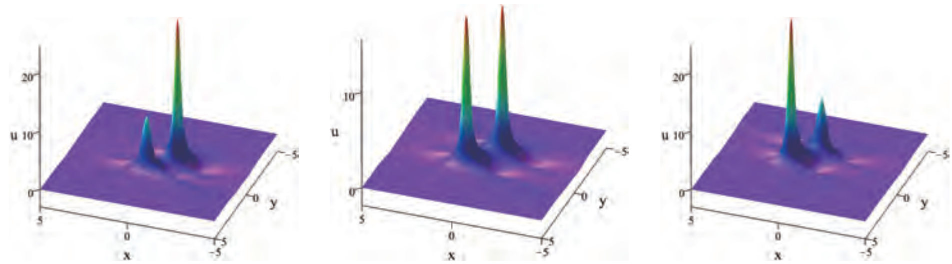

(a) (b) (c)

Fig. 8. (Color online) The time evolution of the two-lump solution from (45) and (9) at (a) $t = -4$; (b) $t = 0$; (c) $t = 4$.

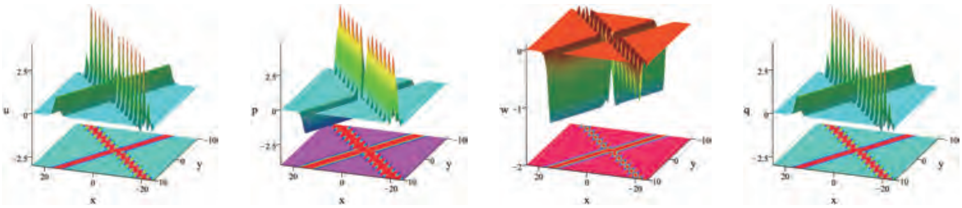

(a) (b) (c) (d)

Fig. 9. (Color online) Interaction solutions between a breather and a line soliton from (46) and (9) in (x, y)-plane.

3.4. *Interaction solution*

In the analysis of interaction solutions for the HSI equation, particular attention is given to the interactions between line and breather, line and lump, and lump and breather solitons. For instance, by setting parameters that adhere to the Hirota bilinear condition, a functional expression for the interaction solution can be derived, revealing a complex interplay among the involved solitons.

Considering the specific parameter settings where $a_1 = a_2^* = \nu_{1R} + \mathrm{I}\nu_{1I}$, $a_3 = \nu_3$, $b_1 = b_2 = \omega_1$, $b_3 = \omega_3$, $c_1 = c_2^* = \nu_{1R} + \mathrm{I}\nu_{1I}$, $c_3 = \nu_3$, and $\eta_1^0 = \eta_2^0 = \eta_3^0 = 0$, while satisfying the Hirota N-soliton condition, the function in (32) can be written as follows:

$$f = 1 + 2\mathrm{e}^{\zeta_1}\cos\vartheta_1 + A_{12}\mathrm{e}^{2\zeta_1} + \mathrm{e}^{\zeta_3}(1 + 2M_1\mathrm{e}^{\zeta_1}\cos(\vartheta_1 + \omega_1) + A_{12}M_1^2\mathrm{e}^{2\zeta_1}), \tag{46}$$

where

$$A_{13} = M_1\mathrm{e}^{\mathrm{I}\omega}, \quad A_{23} = A_{13}^* = M_1\mathrm{e}^{-\mathrm{I}\omega}. \tag{47}$$

By setting $\nu_{1R} = 1$, $\nu_{1I} = 2$, $\nu_3 = \frac{3}{2}$, $\omega_1 = 2$, and $\omega_3 = -2$, an interaction solution between a line and a breather is obtained, as demonstrated in Fig. 9. This interaction results in the line soliton propagating along the breather, as illustrated in Fig. 10.

Given the conditions where $a_1 = a_2^* = \nu_{1R} + \mathrm{I}\nu_{1I}$, $a_3 = \nu_3$, $a_4 = \nu_4$, $b_1 = b_2 = \omega_1$, $b_3 = \omega_3$, $b_4 = \omega_4$, $c_1 = c_2^* = \nu_{1R} + \mathrm{I}\nu_{1I}$, $c_3 = \nu_3$, $c_4 = \nu_4$, and $\eta_1^0 = \eta_2^0 = \eta_3^0 = \eta_4^0 = 0$,

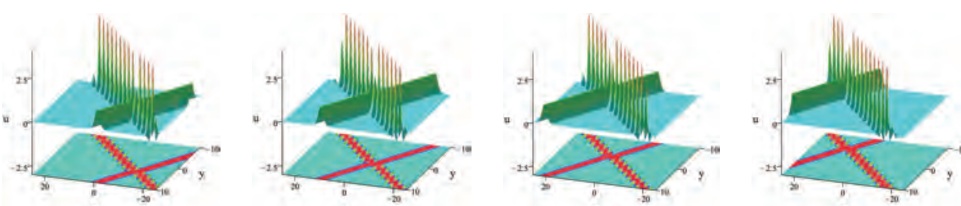

(a) (b) (c) (d)

Fig. 10. (Color online) The time evolution of interaction solution u between a breather and a line soliton from (46) and (9) at (a) $t = -15$; (b) $t = -5$; (c) $t = 5$; (d) $t = 15$.

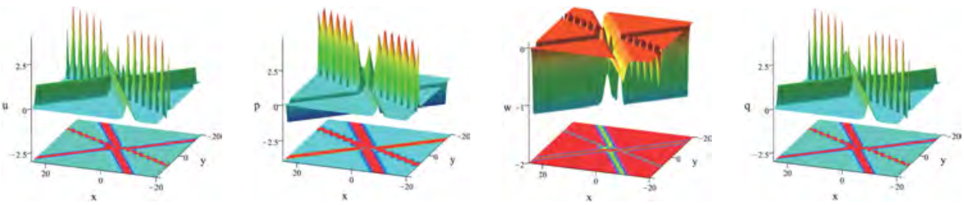

(a) (b) (c) (d)

Fig. 11. (Color online) The interaction solutions between a breather and a two-line soliton from (48) and (9) in the (x, y)-plane.

while satisfying the Hirota N-soliton condition, the function in (33) can be expressed as follows:

$$\begin{aligned} f = &\, 1 + 2e^{\zeta_1}\cos\vartheta_1 + e^{\zeta_3} + e^{\zeta_4} + A_{12}e^{2\zeta_1} + 2M_1 e^{\zeta_1+\zeta_3}\cos(\vartheta_1 + \omega_1) \\ &+ 2M_2 e^{\zeta_1+\zeta_4}\cos(\vartheta_1+\omega_2) + A_{34}e^{\zeta_3+\zeta_4} + A_{12}M_1^2 e^{2\zeta_1+\zeta_3} + A_{12}M_2^2 e^{2\zeta_1+\zeta_3} \\ &+ 2A_{34}M_1M_2 e^{\zeta_1+\zeta_3+\zeta_4}\cos\vartheta_1 + A_{12}A_{34}M_1^2M_2^2 e^{2\zeta_1+\zeta_3+\zeta_4}, \end{aligned} \tag{48}$$

with

$$A_{13} = M_1 e^{I\omega_1}, \quad A_{23} = A_{13}^* = M_1 e^{-I\omega_1}, \quad A_{14} = M_2 e^{I\omega_2}, \quad A_{24} = A_{14}^* = M_2 e^{-I\omega_2}. \tag{49}$$

To illustrate, setting $\nu_{1R} = 1$, $\nu_{1I} = 2$, $\nu_3 = \frac{3}{2}$, $\nu_4 = \frac{3}{2}$, $\omega_1 = 2$, $\omega_3 = -2$, and $\omega_4 = 1$, yields an interaction solution involving a two-line soliton and a breather, depicted in Fig. 11.

In Eq. (32), with specific parameter settings such as $a_1 = l_1\varepsilon$, $a_2 = l_2\varepsilon$, $b_i = m_i a_i$, $c_i = n_i a_i$, $\eta_1^0 = \eta_2^0 = I\pi$, $\eta_3^0 = 0$ $(i = 1, 2, 3)$ $\alpha = 1$, $\beta = 1$, $a_1 = a_2 = a_3 = 1$, $m_1 = m_2^* = 1 + 2I$, $m_3 = 3$, $n_1 = n_2 = n_3 = 1$, and taking the limit as $\varepsilon \to 0$ yields

$$\begin{aligned} f = &\,(\varpi_{12} + \chi_1\chi_2)l_1l_2\varepsilon^2 + (\chi_1\chi_2 + \varpi_{23}\chi_1 + \varpi_{13}\chi_2 + \varpi_{12} + \varpi_{13}\varpi_{23}) \\ &\cdot \exp(\eta_3)l_1l_2\varepsilon^2 + O(\varepsilon^3), \end{aligned} \tag{50}$$

indicating an interaction solution between a lump and a line soliton. The dynamic evolution of this interaction over time is depicted in Fig. 12 on the (x, y)-plane.

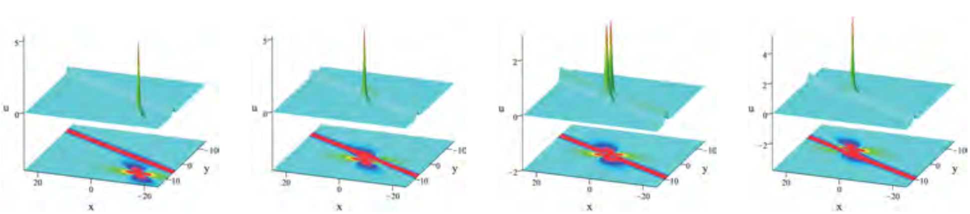

(a) (b) (c) (d)

Fig. 12. (Color online) The time evolution of interaction solution u between a lump and a line soliton from (50) and (9) at (a) $t = -35$; (b) $t = -5$; (c) $t = 5$; (d) $t = 15$.

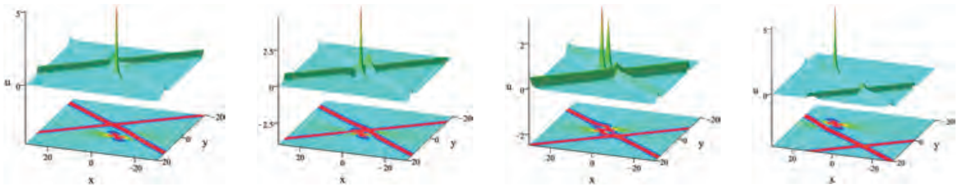

(a) (b) (c) (d)

Fig. 13. (Color online) The time evolution of interaction solution u between a lump and two-line soliton from (51) and (9) at (a) $t=-10$; (b) $t=-5$; (c) $t=5$; (d) $t=30$.

Moving on to Eq. (33), by adopting parameters such as $a_1=l_1\varepsilon,\ a_2=l_2\varepsilon,$ $b_i=m_ia_i,\ \ c_i=n_ia_i,\ \ \eta_1^0=\eta_2^0=\mathrm{I}\pi,\ \ \eta_3^0=\eta_4^0=0\ \ (i=1,2,3,4)\ \ \alpha=1,\ \ \beta=1,$ $a_1=a_2=a_3=a_4=1,\ \ m_1=m_2^*=1+2\mathrm{I},\ \ m_3=2,\ \ m_4=-2,\ \ n_1=n_2=n_3=n_4=1$, and again taking the limit as $\varepsilon\to 0$ yields

$$\begin{aligned} f=&l_1l_2\varepsilon^2[(\varpi_{12}+\chi_1\chi_2)+(\chi_1\chi_2+\varpi_{23}\chi_1+\varpi_{13}\chi_2+\varpi_{12}+\varpi_{13}\varpi_{23})\exp(\eta_3)\\ &+(\chi_1\chi_2+\varpi_{24}\chi_1+\varpi_{14}\chi_2+\varpi_{12}+\varpi_{14}\varpi_{24})\exp(\eta_4)+\varpi_{34}\exp(\eta_3+\eta_4)\\ &\times(\chi_1\chi_2+(\varpi_{23}+\varpi_{24})\chi_1+(\varpi_{13}+\varpi_{14})\chi_2+\varpi_{12}\\ &+(\varpi_{13}+\varpi_{14})(\varpi_{23}+\varpi_{24}))]+O(\varepsilon^3), \end{aligned} \tag{51}$$

indicating an interaction solution between a lump and two-line solitons. The dynamic progression of this interaction is presented in Fig. 13 on the (x,y)-plane.

Furthermore, still considering Eq. (33), taking $a_1=l_1\varepsilon,\ a_2=l_2\varepsilon,\ b_i=m_ia_i,$ $c_i=n_ia_i,\ \eta_1^0=\eta_2^0=\mathrm{I}\pi,\ \eta_3^0=\eta_4^0=0\ (i=1,2,3,4),\ \alpha=1,\ \beta=1,\ a_1=a_2=a_3=a_4=1,\ m_1=m_2^*=1+\frac{5}{2}\mathrm{I},\ m_3=m_4^*=1+3\mathrm{I},\ n_1=n_2=n_3=n_4=1$, and taking the limit as $\varepsilon\to 0$ yields

$$\begin{aligned} f=&l_1l_2\varepsilon^2[(\varpi_{12}+\chi_1\chi_2)+(\chi_1\chi_2+\varpi_{23}\chi_1+\varpi_{13}\chi_2+\varpi_{12}+\varpi_{13}\varpi_{23})\exp(\eta_3)\\ &+(\chi_1\chi_2+\varpi_{24}\chi_1+\varpi_{14}\chi_2+\varpi_{12}+\varpi_{14}\varpi_{24})\exp(\eta_4)+\varpi_{34}\exp(2\zeta_2)\\ &\times(\chi_1\chi_2+(\varpi_{23}+\varpi_{24})\chi_1+(\varpi_{13}+\varpi_{14})\chi_2+\varpi_{12}\\ &+(\varpi_{13}+\varpi_{14})(\varpi_{23}+\varpi_{24}))]+O(\varepsilon^3), \end{aligned} \tag{52}$$

depicting an interaction solution between a lump and a breather, as depicted in Fig. 14 on (x,y)-plane.

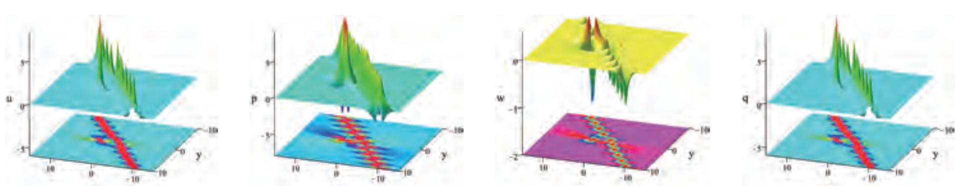

(a) (b) (c) (d)

Fig. 14. (Color online) The interaction solutions between a breather and a lump from (52) and (9).

These analyses provide valuable insights into the elastic interactions between various soliton within the studied framework, shedding light on the complex dynamics inherent in these systems.

4. Multi-Rogue Wave Solutions

Zhaqilao proposed a method in Ref. 41 for generating multi-rogue waves. This approach enables the control of dynamical behavior via a central point (θ, δ), facilitating the exploration of multi-rogue wave solutions for various NPDEs.[42–48] The symbolic computation process for deriving multi-rogue wave solutions generally involves the following steps:

(1) Begin with an NPDE in its general form

$$\mathcal{N}(x, y, z, t, u, u_x, u_y, u_z, u_t, u_{xx}, u_{xy}, u_{xz}, \ldots) = 0. \tag{53}$$

(2) Perform a traveling wave transformation $\xi = x + by - dt$, and through a variable transformation $u = \mathcal{P}(f)$, Eq. (53) is transformed into a bilinear equation in terms of

$$P(D_\xi, D_z) f \cdot f = 0. \tag{54}$$

(3) Assume a specific form for the solution function f, denoted as

$$f = f_{n+1}(\xi, z; \theta, \delta) = A_{n+1}(\xi, z) + 2\theta z B_n(\xi, z) + 2\delta\xi C_n(\xi, z) + (\theta^2 + \delta^2) A_{n-1}(\xi, z), \tag{55}$$

and

$$\begin{aligned} A_n(\xi, z) &= \sum_{k=0}^{n(n+1)/2} \sum_{i=0}^{k} a_{n(n+1)-2k,2i} z^{2i} \xi^{n(n+1)-2k}, \\ B_n(\xi, z) &= \sum_{k=0}^{n(n+1)/2} \sum_{i=0}^{k} b_{n(n+1)-2k,2i} z^{2i} \xi^{n(n+1)-2k}, \\ C_n(\xi, z) &= \sum_{k=0}^{n(n+1)/2} \sum_{i=0}^{k} c_{n(n+1)-2k,2i} z^{2i} \xi^{n(n+1)-2k}, \end{aligned} \tag{56}$$

with $A_0 = 1$, $A_{-1} = B_0 = C_0 = 0$, where $a_{m,l}, b_{m,l}, c_{m,l}$ $(m, l \in \{0, 2, 4, \ldots, n(n+1)\})$, θ and δ are the real amounts.

(4) Appending (55) and (56) to (54), coefficients of various powers of ξ and z are collected, and through straightforward algebraic manipulations, the coefficients $a_{m,l}$, $b_{m,l}$, and $c_{m,l}$ are obtained.

(5) Upon obtaining the coefficients $a_{m,l}$, $b_{m,l}$, and $c_{m,l}$, substitute them back into $u = \mathcal{P}(f)$ to derive the multi-rogue wave solutions for (53).

In the context of the $(3+1)$-dimensional HSI equation (8), a traveling wave transformation $\xi = x + by - dt$ is performed, resulting in the following form:

$$\begin{cases} \alpha(-d)p_\xi + (-d)u_{\xi\xi\xi} + 3(uw)_\xi + \beta q_z = 0, \\ (-d)u_\xi = w_\xi, \quad bu_\xi = p_\xi, \quad u_z = q_\xi. \end{cases} \tag{57}$$

This transformation leads to the dependent variable transformations

$$u = 2(\ln f)_{\xi\xi}, \quad p = 2b(\ln f)_{\xi\xi}, \quad w = 2(-d)(\ln f)_{\xi\xi}, \quad q = 2(\ln f)_{\xi z}, \tag{58}$$

resulting in the bilinear form of Eq. (57)

$$(-\alpha bdD_\xi^2 - dD_\xi^4 + \beta D_z^2)f \cdot f = 0. \tag{59}$$

When $n = 0$, Eq. (55) can be rewritten as follows:

$$\begin{aligned} f &= f_1(\xi, z; \theta, \delta) = A_1(\xi, z) + 2\theta z B_0(\xi, z) + 2\delta\xi C_0(\xi, z) + (\theta^2 + \delta^2)A_{-1}(\xi, z) \\ &= a_{0,0} + a_{0,2}z^2 + a_{2,0}\xi^2. \end{aligned} \tag{60}$$

To simplify, let's choose $a_{2,0} = 1$ and substitute Eq. (60) into Eq. (59). By setting the coefficients of all powers of ξ and z to zero, we find: $a_{0,0} = -\frac{3}{\alpha b}$ and $a_{0,2} = -\frac{\alpha bd}{\beta}$. Thus, Eq. (60) transforms into

$$f = f_1(\xi, z; \theta, \delta) = (\xi - \theta)^2 - \frac{\alpha bd}{\beta}(z - \delta)^2 - \frac{3}{\alpha b}. \tag{61}$$

To preclude singularities, it is imperative that (61) remains a positive quadratic polynomial.[49,50] Applying the transformation given in Eq. (58), the one-rogue wave solutions take the following form:

$$\begin{aligned} u &= -\frac{8[(\xi-\theta)^2 + \frac{\alpha bd}{\beta}(z-\delta)^2 + \frac{3}{\alpha b}]}{[(\xi-\theta)^2 - \frac{\alpha bd}{\beta}(z-\delta)^2 - \frac{3}{\alpha b}]^2}, \\ p &= -\frac{8b[(\xi-\theta)^2 + \frac{\alpha bd}{\beta}(z-\delta)^2 + \frac{3}{\alpha b}]}{[(\xi-\theta)^2 - \frac{\alpha bd}{\beta}(z-\delta)^2 - \frac{3}{\alpha b}]^2}, \\ w &= \frac{8d[(\xi-\theta)^2 + \frac{\alpha bd}{\beta}(z-\delta)^2 + \frac{3}{\alpha b}]}{[(\xi-\theta)^2 - \frac{\alpha bd}{\beta}(z-\delta)^2 - \frac{3}{\alpha b}]^2}, \\ q &= \frac{8\frac{\alpha bd}{\beta}(\xi-\theta)(z-\delta)}{[(\xi-\theta)^2 - \frac{\alpha bd}{\beta}(z-\delta)^2 - \frac{3}{\alpha b}]^2}. \end{aligned} \tag{62}$$

This rogue exhibits the following characteristics:

$$\lim_{\xi\to\pm\infty} u_{\xi,z} = 0, \qquad \lim_{z\to\pm\infty} u_{\xi,z} = 0. \tag{63}$$

For $\alpha = -1$, $\beta = 3$, $b = 1$, $d = 1$, $\delta = \theta = 0$, it is confirmed that f in (61) is a positive quadratic polynomial. The one-rogue wave solutions are illustrated in Fig. 15, with the wave center located at $(0, 0)$ if $\theta \neq 0$ and $\delta \neq 0$, the center shifts to (θ, δ). After

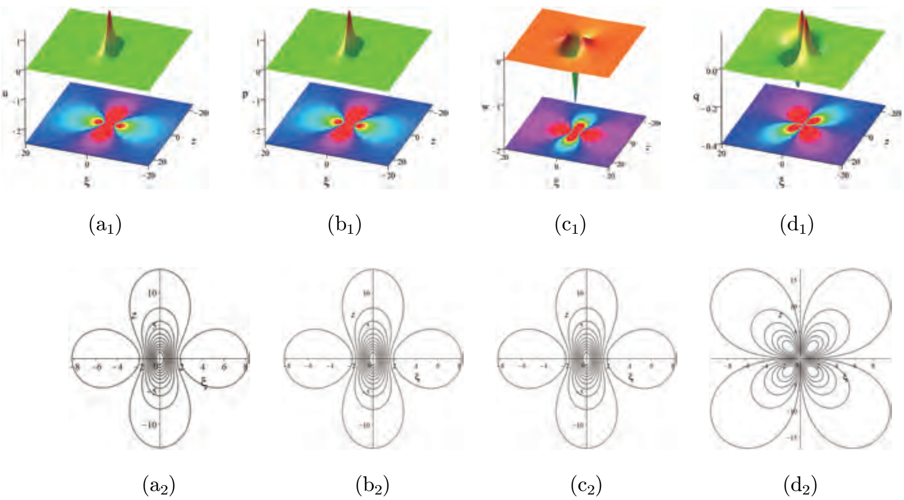

Fig. 15. (Color online) One-rogue wave solutions (61) with $\alpha=-1$, $\beta=3$, $b=1$, $d=1$, $\delta=\theta=0$.

calculation, the following values are obtained:

$$\begin{aligned} &u(0,0)=\frac{4}{3}, \quad u(3,0)=-\frac{1}{6}, \quad u(-3,0)=-\frac{1}{6};\\ &p(0,0)=\frac{4}{3}, \quad p(3,0)=-\frac{1}{6}, \quad p(-3,0)=-\frac{1}{6};\\ &w(0,0)=-\frac{4}{3}, \quad w(3,0)=\frac{1}{6}, \quad w(-3,0)=\frac{1}{6};\\ &q\left(\frac{\sqrt{6}}{2},\frac{3\sqrt{2}}{2}\right)=-\frac{\sqrt{3}}{9}, \quad q\left(-\frac{\sqrt{6}}{2},-\frac{3\sqrt{2}}{2}\right)=-\frac{\sqrt{3}}{9},\\ &q\left(-\frac{\sqrt{6}}{2},\frac{3\sqrt{2}}{2}\right)=\frac{\sqrt{3}}{9}, \quad q\left(\frac{\sqrt{6}}{2},-\frac{3\sqrt{2}}{2}\right)=\frac{\sqrt{3}}{9}. \end{aligned} \tag{64}$$

As depicted in Fig. 15, the components u and p represent rogues with peaks facing upward, while w represents a rogue with troughs facing upward. On the other hand, the component q exhibits a double-peaked structure. The upper layer displays 3D and density plots, while the lower layer shows contour plots.

When $n=1$, Eq. (55) can be rewritten as follows:

$$\begin{aligned} f&=f_2(\xi,z;\theta,\delta)=A_2(\xi,z)+2\theta zB_1(\xi,z)+2\delta\xi C_1(\xi,z)+(\theta^2+\delta^2)A_0(\xi,z)\\ &=(a_{0,0}+a_{0,2}z^2+a_{0,4}z^4+a_{0,6}z^6)+(a_{2,0}+a_{2,2}z^2+a_{2,4}z^4)\xi^2\\ &\quad+(a_{4,0}+a_{4,2}z^2)\xi^4+a_{6,0}\xi^6+2\theta z(b_{0,0}+b_{0,2}z^2+b_{2,0}\xi^2)\\ &\quad+2\delta\xi(c_{0,0}+c_{0,2}z^2+c_{2,0}\xi^2)+(\theta^2+\xi^2). \end{aligned} \tag{65}$$

To simplify, let's choose $a_{6,0} = 1$ and substitute Eq. (65) into Eq. (59). By setting the coefficients of all powers of ξ and z to zero, we find

$$\begin{aligned}
a_{0,0} &= \frac{9\alpha^3 b^3 d((c_{2,0}^2 - 1)\delta^2 - \theta^2) - \alpha^2\beta b^2 b_{2,0}^2\theta^2 - 16875d}{9\alpha^3 b^3 d}, \\
a_{0,2} &= -\frac{475d}{\alpha\beta b}, \quad a_{0,4} = -\frac{17\alpha b d^2}{\beta^2}, \quad a_{0,6} = -\frac{\alpha^3 b^3 d^3}{\beta^3}, \quad a_{2,0} = -\frac{125}{\alpha^2 b^2}, \\
a_{2,2} &= \frac{90d}{\beta}, \quad a_{2,4} = \frac{3\alpha^2 b^2 d}{\beta^2}, \quad a_{4,0} = \frac{25}{\alpha b}, \quad a_{4,2} = -\frac{3\alpha b d}{\beta}, b_{0,0} = -\frac{5b_{2,0}}{3\alpha b}, \\
b_{0,2} &= -\frac{\alpha b d b_{2,0}}{3\beta}, \quad b_{2,0} = b_{2,0}, \quad c_{0,0} = \frac{c_{2,0}}{\alpha b}, \quad c_{0,2} = \frac{3\alpha b d c_{2.0}}{\beta}, \quad c_{2,0} = c_{2,0}.
\end{aligned} \tag{66}$$

Substituting (65) and (66) into (58), the two-rogue wave solutions are derived. For $\alpha = -1$, $\beta = 3$, $b = 1$, $d = 2$, $b_{2,0} = 1$, $c_{2,0} = 2$. When $\delta = \theta = 0$, the two-rogue wave concentrates near $(0, 0)$, as shown in Fig. 16(a); for $\delta = \theta = 50$, it can be observed that the two-rogue wave is undergoing splitting, depicted in Fig. 16(b); when $\delta = \theta = 500$, the two-rogue wave splits into three one-rogue waves, depicted in

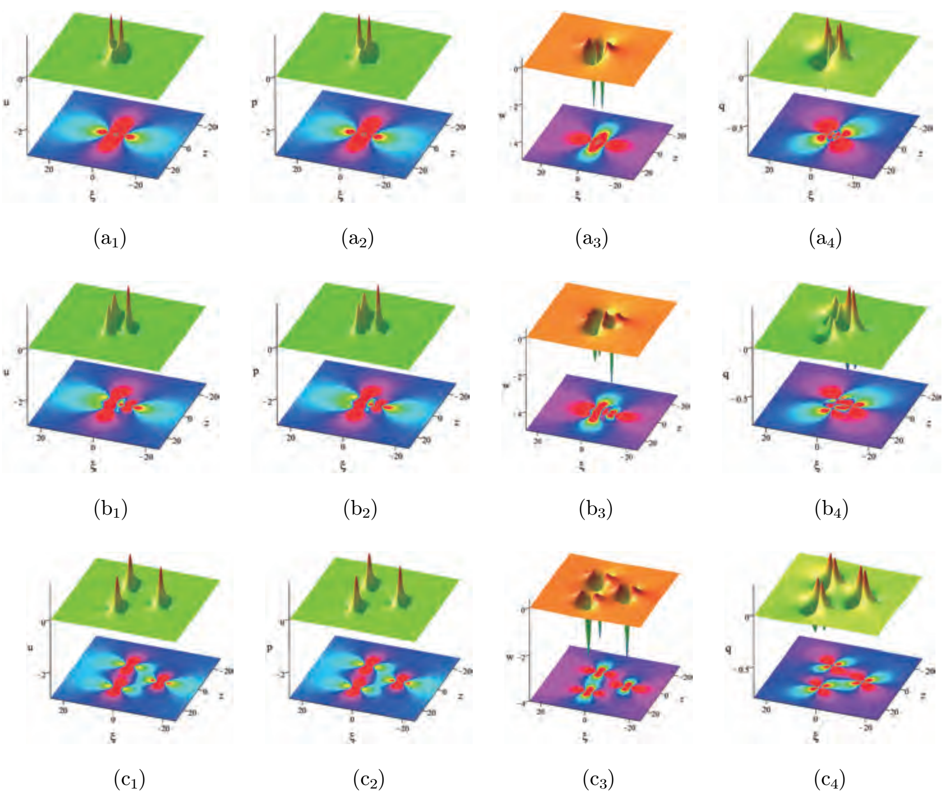

Fig. 16. (Color online) Two-rogue wave solutions (65) with $\alpha = -1$, $\beta = 3$, $b = 1$, $d = 2$, $c_{2,0} = 2$, $b_{2,0} = 1$. The parameters are (a$_1$)–(a$_4$) $\delta = \theta = 0$; (b$_1$)–(b$_4$) $\delta = \theta = 50$; (c$_1$)–(c$_4$) $\delta = \theta = 500$.

Fig. 16(c). That is, when δ and θ are sufficiently large, the two-rogue wave can consist of at most three one-rogue waves, forming a triangle.

When $n = 2$, Eq. (55) can be rewritten as follows:

$$\begin{aligned} f = f_3(\xi, z; \theta, \delta) &= A_3(\xi, z) + 2\theta z B_2(\xi, z) + 2\delta\xi C_2(\xi, z) + (\theta^2 + \delta^2)A_1(\xi, z) \\ &= (a_{0,0} + a_{0,2}z^2 + a_{0,4}z^4 + a_{0,6}z^6 + a_{0,8}z^8 + a_{0,10}z^{10} + a_{0,12}z^{12}) + (a_{2,0} \\ &\quad + a_{2,2}z^2 + a_{2,4}z^4 + a_{2,6}z^6 + a_{2,8}z^8 + a_{2,10}z^{10})\xi^2 + (a_{4,0} + a_{4,2}z^2 + a_{4,4}z^4 \\ &\quad + a_{4,6}z^6 + a_{4,8}z^8)\xi^4 + (a_{6,0} + a_{6,2}z^2 + a_{6,4}z^4 + a_{6,6}z^6)\xi^6 + (a_{8,0} + a_{8,2}z^2 \\ &\quad + a_{8,4}z^4)\xi^8 + (a_{10,0} + a_{10,2}z^2)\xi^{10} + a_{12,0}\xi^{12} + 2\theta z((b_{0,0} + b_{0,2}z^2 + b_{0,4}z^4 \\ &\quad + b_{0,6}z^6) + (b_{2,0} + b_{2,2}z^2 + b_{2,4}z^4)\xi^2 + (b_{4,0} + b_{4,2}z^2)\xi^4 + b_{6,0}\xi^6) \\ &\quad + 2\delta\xi((c_{0,0} + c_{0,2}z^2 + c_{0,4}z^4 + c_{0,6}z^6) + (c_{2,0} + c_{2,2}z^2 + c_{2,4}z^4)\xi^2 \\ &\quad + (c_{4,0} + c_{4,2}z^2)\xi^4 + c_{6,0}\xi^6) + (\theta^2 + \delta^2)\left(-\frac{\alpha b d z^2}{\beta} + \xi^2 - \frac{3}{\alpha b}\right). \end{aligned} \tag{67}$$

Substitute Eq. (67) into Eq. (59). By setting the coefficients of all powers of ξ and z to zero, we find

$$\begin{aligned} a_{0,0} &= \frac{17334a_{4,4}\alpha^5 b^5 \beta d^2(\delta^2 + \theta^2) + 25966332\alpha^4 b^4 b_{6,0}^2 d^3\theta^2}{5778a_{4,4}\beta d^2\alpha^6 b^6} \\ &\quad + \frac{-8014300\alpha^3 b^3 \beta c_{4,2}^2 d^2\delta^2 + 15065589a_{4,4}^2\beta^2}{5778a_{4,4}\beta d^2\alpha^6 b^6}, \\ a_{0,2} &= \frac{8667a_{4,4}\alpha^5 b^5 \beta d^2(\delta^2 + \theta^2) + 12983166\alpha^4 b^4 b_{6,0}^2 d^3\theta^2}{8667a_{4,4}\beta^2 d\alpha^4 b^4} \\ &\quad + \frac{-4007150\alpha^3 b^3 \beta c_{4,2}^2 d^2\delta^2 + 23212005a_{4,4}^2\beta^3}{8667a_{4,4}\beta^2 d\alpha^4 b^4}, \\ a_{0,4} &= \frac{93667a_{4,4}}{642\alpha^2 b^2}, \quad a_{0,6} = a_{0,6}, \quad a_{0,8} = \frac{867a_{4,4}\alpha^2 b^2 d^2}{7490\beta^2}, \\ a_{0,10} &= \frac{29\alpha^4 b^4 d^3 a_{4,4}}{18725\beta^3}, \quad a_{0,12} = \frac{a_{4,4}d^4\alpha^6 b^6}{37450\beta^4}, \\ a_{2,0} &= -\frac{8667a_{4,4}\alpha^5 b^5 \beta d^2(\delta^2 + \theta^2) + 12983166\alpha^4 b^4 b_{6,0}^2 d^3\theta^2}{8667a_{4,4}\beta d^2\alpha^5 b^5} \\ &\quad - \frac{-4007150\alpha^3 b^3 \beta c_{4,2}^2 a^2\delta^2 + 12326391a_{4,4}^2\beta^3}{8667a_{4,4}\beta d^2\alpha^5 b^5}, \\ a_{2,2} &= -\frac{1617\beta a_{4,4}}{107d\alpha^3 b^3}, \quad a_{2,4} = \frac{42a_{4,4}}{107\alpha b}, \quad a_{2,6} = -\frac{506a_{4,4}\alpha b d}{535\beta}, \\ a_{2,8} &= -\frac{57\alpha^3 b^3 d^2 a_{4,4}}{3745\beta^2}, \quad a_{2,10} = -\frac{3a_{4,4}d^3\alpha^5 b^5}{18725\beta^3}, \quad a_{4,0} = -\frac{29645a_{4,4}\beta^2}{642d^2\alpha^4 b^4}, \\ a_{4,2} &= \frac{630\beta a_{4,4}}{107\alpha^2 b^2 d}, \quad a_{4,6} = \frac{146\alpha^2 d b^2 a_{4,4}}{3745\beta}, \quad a_{4,8} = \frac{3a_{4,4}d^2\alpha^4 b^4}{7490\beta^2}, \\ a_{6,0} &= -\frac{1078a_{4,4}\beta^2}{1605d^2\alpha^3 b^3}, \quad a_{6,2} = -\frac{266\beta a_{4,4}}{535\alpha b d}, \quad a_{6,4} = -\frac{22\alpha b a_{4,4}}{535}, \end{aligned}$$

$$
\begin{aligned}
a_{6,6} &= -\frac{2a_{4,4}d\alpha^3b^3}{3745\beta}, \quad a_{8,0} = \frac{21a_{4,4}\beta^2}{1070\alpha^2b^2d^2}, \quad a_{8,2} = \frac{69\beta a_{4,4}}{3745d}, \\
a_{8,4} &= \frac{3a_{4,4}\alpha^2b^2}{7490}, \quad a_{10,0} = -\frac{7a_{4,4}\beta^2}{2675d^2\alpha b}, \quad a_{10,2} = -\frac{3a_{4,4}\beta\alpha b}{18725d}, \\
a_{12,0} &= \frac{a_{4,4}\beta^2}{37450d^2}, \quad b_{0,0} = -\frac{3773b_{6,0}}{3\alpha^3b^3}, b_{0,2} = \frac{49db_{6,0}}{\beta\alpha b}, \quad b_{0,4} = \frac{7\alpha bd^2b_{6,0}}{5\beta^2}, \\
b_{0,6} &= -\frac{\alpha^3b^3b_{6,0}d^3}{5\beta^3}, \quad b_{2,0} = -\frac{133b_{6,0}}{\alpha^2b^2}, \quad b_{2,4} = -\frac{9\alpha^2b^2b_{6,0}d^2}{5\beta^2}, \quad b_{4,0} = -\frac{21b_{6,0}}{\alpha b}, \\
b_{4,2} &= \frac{\alpha bb_{6,0}d}{\beta}, \quad b_{6,0} = b_{6,0}, \quad c_{0,0} = -\frac{12005\beta c_{4,2}}{27d\alpha^4b^4}, \quad c_{0,2} = -\frac{535c_{4,2}}{9\alpha^2b^2}, \\
c_{0,4} &= -\frac{5dc_{4,2}}{\beta}, \quad c_{0,6} = -\frac{5\alpha^2b^2c_{4,2}d^2}{9\beta^2}, \quad c_{2,0} = -\frac{245\beta c_{4,2}}{9d\alpha^3b^3}, \quad c_{2,2} = -\frac{230c_{4,2}}{9\alpha b}, \\
c_{2,4} &= -\frac{5\alpha bc_{4,2}d}{9\beta}, \quad c_{4,0} = -\frac{13\beta c_{4,2}}{9\alpha^2b^2d}, \quad c_{4,2} = c_{4,2}, \quad c_{6,0} = \frac{\beta c_{4,2}}{9\alpha bd}.
\end{aligned}
\tag{68}
$$

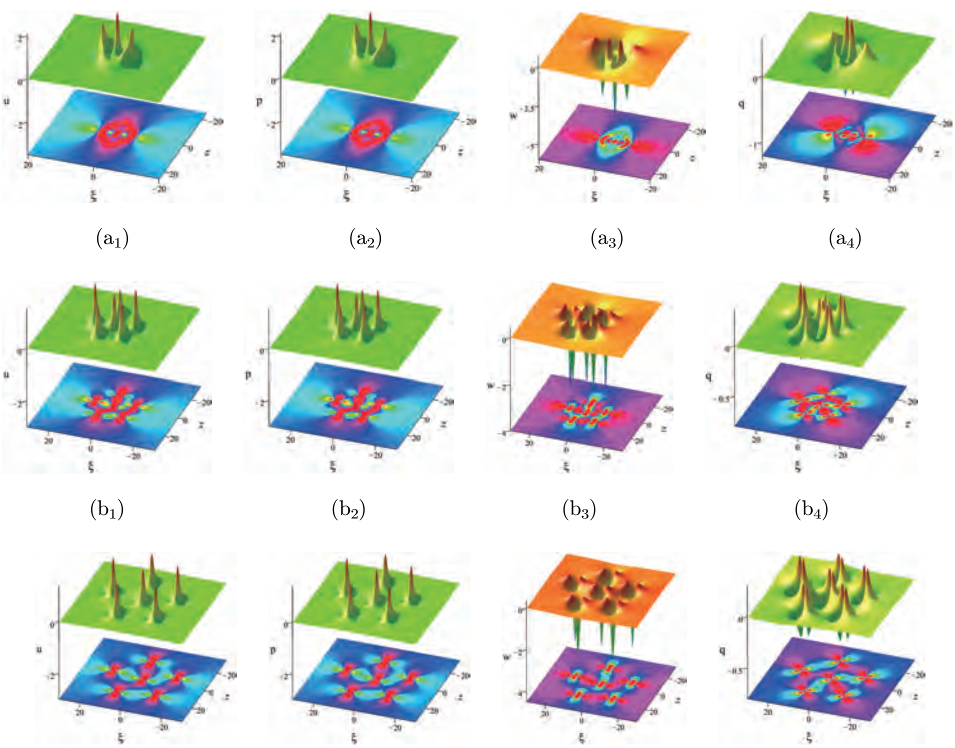

(a$_1$) (a$_2$) (a$_3$) (a$_4$)

(b$_1$) (b$_2$) (b$_3$) (b$_4$)

(c$_1$) (c$_2$) (c$_3$) (c$_4$)

Fig. 17. (Color online) Three-rogue wave solutions (67) with $\alpha = -1$, $\beta = 3$, $b = 1$, $d = 2$, $a_{4,4} = 2$, $b_{6,0} = 1$, $c_{4,2} = 1$. The parameters are (a$_1$)–(a$_4$) $\delta = \theta = 0$; (b$_1$)–(b$_4$) $\delta = \theta = 50$; (c$_1$)–(c$_4$) $\delta = \theta = 500$.

Substituting (67) and (68) into (58), the three-rogue wave solutions are derived. For $\alpha=-1,\ \beta=3,\ b=1,\ d=2,\ a_{4,4}=2,\ b_{6,0}=1,\ c_{4,2}=1$. Similarly, as δ and θ gradually increase, the three-rogue starts splitting from the center $(0,0)$, eventually forming a three-rogue wave consisting of a central peak and five peaks around it, forming a ring-like structure, as Fig. 17.

Comparing the N-lump from the long-wave limit and the N-rogue wave from multiple-rogue wave method, we observe that the former consists of N lumps, while the latter is composed of $\frac{N(N+1)}{2}$ rogues controlled by the wave center (θ,δ). Furthermore, the former undergoes elastic collisions over time, whereas the latter exhibits fixed patterns, such as a triangle, a pentagon, and so forth.

5. Conclusions

In this paper, the dynamic behavior of the $(3+1)$-dimensional HSI equation (8) is explored. The Hirota N-soliton conditions were examined to ascertain the existence of N-soliton solutions, which elucidate the integrable properties of the equation under specific conditions. The Hirota bilinear method was applied to derive soliton solutions (see Figs. 1 and 2) ranging from one-soliton to four-soliton solutions for the HSI equation (8). These solutions exhibit various shapes, including bell and anti-bell shapes, due to the equation's four components u, p, w, and q. Moreover, by introducing complex conjugate parameters, breather solutions (see Figs. 3–5) were obtained, including one breather and two-breather, which manifest differently across different planes. For instance, a one breather in the (x,t)-plane represents the classical breather, while in the $(x$–$z)$-plane, it exhibits two periodic waveform modes. Additionally, utilizing the long-wave limit technique, we derived lump solutions (see Figs. 6–8), including one lump and two-lump. Similarly, one lump in the (y,z)-plane resembles the classical lump, but in the (x,z)-plane, it transforms into a line-lump. The two lumps demonstrates elastic collisions. Furthermore, three types of interaction solutions (see Figs. 9–14) were explored, namely breather and line, lump and line, and breather and lump interactions, analyzing their temporal evolution behavior. Additionally, employing multiple-rogue wave method, multi-rogue wave solutions of the HSI equation (8) for $n=0,1,2$ (see Figs. 15–17) were obtained, controlled by the wave center (θ,δ). As the wave center (θ,δ) varies, multi-rogue waves eventually exhibit aesthetically pleasing patterns, such as triangles, centered pentagons. These findings deepen our understanding of the dynamics and behavior of the HSI equation, paving the way for further exploration in nonlinear wave phenomena and integrable systems.

Acknowledgments

The authors would like to thank the referees for the constructive comments. This work is supported by the Beijing Natural Science Foundation (No. 1222005).

ORCID

Jingyi Chu https://orcid.org/0009-0003-6299-0003
Yaqing Liu https://orcid.org/0000-0001-6354-5401
Wen-Xiu Ma https://orcid.org/0000-0003-4097-1621

References

1. M. J. Ablowitz, P. A. Clarkson, *Solitons, Nonlinear Evolution Equations and Inverse Scattering* (Cambridge University Press, United Kingdom, 1991).
2. M. J. Ablowitz and Z. H. Musslimani, *Nonlinearity* **29** (2016) 915.
3. M. J. Ablowitz, *Optik* **278** (2023) 170710.
4. Y. Q. Liu, W. X. Zhang and W. X. Ma, *Commun. Nonlinear Sci. Numer. Simul.* **118** (2023) 107052.
5. A. A. Bolibrukh, *Russ. Math. Surv.* **45** (1990) 1.
6. P. Deift and X. Zhou, *Bull. Am. Math. Soc.* **26** (1992) 119.
7. P. Deift and X. Zhou, *Ann. Math.* **137** (1993) 295.
8. B. Guo, L. Ling and Q. P. Liu, *Phys. Rev. E* **85** (2012) 026607.
9. L. Liu, X. Y. Wen and D. S. Wang, *Appl. Math. Model.* **67** (2019) 201.
10. R. Hirota, *The Direct Method in Soliton Theory* (Cambridge University Press, United Kingdom, 2004).
11. J. Y. Chu, X. Chen and Y. Q. Liu, *Nonlinear Dyn.* **112** (2024) 619.
12. B. Li, Y. Chen, H. Xuan and H. Zhang, *Chaos Soliton Fractals* **17** (2003) 885.
13. Y. Q. Liu and L. Y. Peng, *Chaos Soliton Fractals* **171** (2023) 113430.
14. H. D. Wahlquist and F. B. Estabrook, *Phys. Rev. Lett.* **31** (1973) 1386.
15. R. Hirota and J. Satsuma, *Prog. Theor. Phys. Suppl.* **59** (1976) 64.
16. S. Y. Lou, X. Hu and Y. Chen, *J. Phys. A, Math. Theor.* **45** (2012) 155209.
17. W. X. Ma and L. H. Lee, *Chaos Soliton Fractals* **42** (2009) 1356.
18. R. Hirota, J. Satsuma, *J. Phys. Soc. Jpn.* **40** (1976) 611.
19. M. Ito, *J. Phys. Soc. Jpn.* **49** (1980) 771.
20. J. Hietarinta, *Lect. Notes Phys.* **495** (1997) 95.
21. Y. Zhou, S. Manukure and W. X. Ma, *Commun. Nonlinear Sci. Numer. Simul.* **68** (2019) 56.
22. Y. N. An and R. Guo, *Nonlinear Dyn.* **111** (2023) 18291.
23. Y. Shen, B. Tian, T. Y. Zhou and X. T. Gao, *Chaos Soliton Fractals* **157** (2022) 111861.
24. W. Liu, A. M. Wazwaz and X. Zheng, *Phys. Scr.* **94** (2019) 075203.
25. Y. Liu, X. Y. Wen and D. S. Wang, *Comput. Math. Appl.* **77** (2019) 947.
26. Z. J. Wu and S. F. Tian, *Math. Comput. Simul.* **210** (2023) 235.
27. X. Chen, Y. Liu and J. Zhuang, *Nonlinear Dyn.* **111** (2023) 10367.
28. B. Wang, Z. Ma and X. Liu, *Eur. Phys. J. D* **76**(9) (2022) 165.
29. A. C. Newell and Z. Yunbo, *J. Math. Phys.* **27** (1986) 2016.
30. J. Hietarinta, *J. Math. Phys.* **28** (1987) 1732.
31. J. Hietarinta, *J. Math. Phys.* **28** (1987) 2094.
32. J. Hietarinta, *J. Math. Phys.* **28** (1987) 2586.
33. J. Hietarinta, *J. Math. Phys.* **29** (1988) 628.
34. W. X. Ma, *Commun. Nonlinear Sci. Numer. Simul.* **16** (2011) 2663.
35. W. X. Ma, *Math. Comput. Simul.* **190** (2021) 270.
36. W. X. Ma, *Partial Differ. Equ. Appl. Math.* **5** (2022) 100220.
37. W. X. Ma, *J. Geom. Phys.* **165** (2021) 104191.
38. W. X. Ma, X. Yong and X. Lü, *Wave Motion* **103** (2021) 102719.

39. W. X. Ma and E. G. Fan, *Comput. Math. Appl.* **61** (2011) 950.
40. W. X. Ma, Y. Zhang, Y. Tang and J. Tu, *Appl. Math. Comput.* **218** (2012) 7174.
41. Q. L. Zha, *Comput. Math. Appl.* **75** (2018) 3331.
42. J. G. Liu and W. H. Zhu, *Chin. J. Phys.* **67** (2020) 492.
43. W. Liu and Y. Zhang, *Z. Angew. Math. Phys.* **70** (2019) 1.
44. W. Liu and Y. Zhang, *Appl. Math. Lett.* **98** (2019) 184.
45. J. Ren, O. A. Ilhan, H. Bulut and J. Manafian, *J. Geom. Phys.* **164** (2021) 104159.
46. J. Zhao, J. Manafian, N. E. Zaya and S. A. Mohammed, *Math. Methods Appl. Sci.* **44** (2021) 5079.
47. Y. Niu, Q. Yuan, B. Ghanbari, Z. Zhang and Y. Cao, *Results Phys.* **56** (2024) 107223.
48. S. Arshed, N. Raz, A. R. Butt, A. Javid and J. F. Gómez-Aguilar, *J. Ocean Eng. Sci.* **8** (2023) 33.
49. W. X. Ma and Y. Zhou, *J. Differ. Equ.* **264** (2018) 2633.
50. W. X. Ma, *Mathematics* **11** (2023) 4664.